Occupant Protection in Far-Side Impacts

Bengt Pipkorn, Karl-Johan Larsson, Daniel Perez Rapela, Craig Markusic, Bryant Whitcomb, Murthy Ayyagari and Cecilia Sunnevång

Abstract The potential injury reducing benefits by a far-side airbag was evaluated by means of human body modelling (HBM). The human body model (HBM) was validated for far side evaluation by means of PMHS tests carried out under six simplified far-side impact conditions. A CORrelation Analysis (CORA) rating was carried out. Based on the CORA score and the proposed biofidelity evaluation procedure the model was considered valid to be used in evaluation of far-side impact countermeasures.

The HBM was thereafter positioned in a sled model developed based on the proposed Euro-NCAP 2020 protocol. The predicted risk of rib fractures and lateral head excursion was evaluated both with and without far-side airbag. The proposed far-side airbag was found to reduce head excursion and rib fracture risk in far-side impacts from 90^0 to 15^0 impact angles.

To assess Euro-NCAP far-side sled test rating performance, a 50%-ile WorldSID crash dummy model was positioned in the sled model. Without countermeasure, the head displacement exceeded the occupant interaction limit. With far-side airbag the head excursion limit was not exceeded. The far-side airbag also reduced chest deflection from above the high-performance limit to below, such that a full score was obtained also for the chest evaluation.

Keywords Far-side, Bag, WorldSID, THUMS, Euro-NCAP

I. INTRODUCTION

Although a substantial percentage of injuries sustained in side crashes result from far-side collision, few vehicles are equipped with countermeasures that can reduce the injury risk. Previous studies have shown that approximately 35% of the side crash-related injuries result from far-side collisions, where the occupant is seated opposite the intruding structure [1]. Furthermore, previous studies have also shown that head and thorax are the most frequently injured body regions [1-3]. Countermeasures that can reduce injury risk and the potential safety benefits of such countermeasures in far-side impacts have also been demonstrated [4-5].

The importance of far-side impact is also acknowledged by Euro-NCAP. In the proposed Euro-NCAP 2020 protocol, a far-side impact test and evaluation protocol are included [6]. According to the protocol, an acceleration-based sled rig is to be used along with a ‘body in white’ (BIW). The BIW shall be mounted with the centreline at 75º ±3º towards the direction of travel. All features that may influence occupant kinematics and protection must be installed in the BIW. One WorldSID 50%-ile male dummy will be seated on the far-side of the vehicle. Two sled tests are required for a complete far-side occupant evaluation. The acceleration pulses to drive the sled rig shall be recorded at the non-struck B-pillar in the rating tests included in the side-impact assessment protocol; 60 km/h AE-MDB (Advanced European Mobile Deformable Barrier) and 32 km/h Pole impact. The pulses shall be scaled before being applied in the sled test. Injury is assessed by head impact criterion (HIC), head acceleration (3 ms), head excursion, neck forces, neck moments, and chest and abdomen compression. Head excursion is assessed by three limits: occupant interaction limit (250 mm laterally inboard from struck side seat centreline); head excursion higher performance limit (at the undeformed struck side seat centreline); and maximum intrusion line, as measured after the respective side-impact test.

B. Pipkorn (e-mail: bengt.pipkorn@autoliv.com; tel: +46 (0)322 626341) is Adjunct Professor at Chalmers University of Technology, Gothenburg, and Director of Simulation and Active Structures at Autoliv Research, Vårgårda, Sweden, where C. Sunnevang is Vice President Research. K. Larsson is a PhD student in Traffic Safety at Chalmers University. D. Perez-Rapela is a PhD Student at University of Virginia, USA. C. Markusic, B. Whitcomb and M. Ayyagari are all Principal Engineers and Technical Experts for Side Crashworthiness at Honda R&D Americas, Inc.

The WorldSID 50%-ile male is the most recent side-impact dummy. However, its biofidelity in far-side conditions has not been thoroughly evaluated. Pintar *et al.* [7] compared WorldSID, Thor-NT and PMHS in a far-side loading condition and found that the kinematics of the WorldSID was similar to the PMHS. However, it was also found that the Thor-NT and WorldSID had difficulties measuring the appropriate chest deformations. One reason for the limited capability to predict rib fractures could be the design of the chest deflection measurement, which was designed for near-side impact injury assessment. Computational human surrogate models have the potential (when properly validated) to predict human kinematics and injury for omnidirectional loading [8]. In the computational human body models (HBMs), the injury risk can be predicted using physical parameters, such as strain for predicting rib fracture risk. A probabilistic method based on predicted strain in the cortical bone of the rib was developed and validated to assess the risk of an occupant sustaining rib fractures [9].

The biofidelity and the capability to predict rib fractures of computational human surrogate models in far-side is also not well understood. Therefore, it is necessary to evaluate the biofidelity of both physical and computational surrogates under far-side impact conditions.

Forman *et al.* [10] performed an extensive parametric study of the influence of restraint conditions on responses of PMHS in simplified far-side impact conditions. This test data can be used for evaluation of the biofidelity of both mechanical and computational human surrogate models. From the Forman *et al*. [10] far-side PMHS studies, a total of six sled test configurations for the HBM biofidelity investigation were carried out (Table I). Varied parameters between the different test configurations were: impact severity (ΔV); impact direction; anterior-posterior position of the seatbelt D-ring; deployment of retractor pre-tensioner; and blocking of the pelvis with a plate attached at the inboard edge of the seat. The common factor in these six test configurations was that there was identical upper limb position at the start of the sled tests (hands on thighs).

TABLE I
PMHS SLED TEST CONFIGURATIONS USED IN BIOFIDELITY INVESTIGATION

Config.	ΔV (km/h)	Impact direction (°)	D-Ring position	Pre-tensioning	Pelvis blocked	PMHS ID	Test ID
1	34	60	Middle	Yes	No	591,602	S0124, S0135
2	16	60	Middle	No	No	591, 602, 608	S0233, S0133, S0136
3	16	60	Middle	Yes	No	591, 602 ,608	S0123, S0134, S0137
4	16	60	Back	Yes	Yes	587	S0129
5	16	90	Forward	Yes	No	551, 559	S0083, S0088
6	34	90	Middle	Yes	No	559	S0091

In all tests, 3D displacement relative to the sled buck was measured with a VICON system for landmarks on the head, left and right acromia, T1 vertebrae and pelvis on each PMHS. The displacements of pelvis and T1 were used to calculate the degree of lateral lean (tilt of the thorax), and the difference in forward excursion between the left and right acromia was used to calculate the degree of torso twist. The belt forces in each test were recorded at the upper shoulder-belt segment, between the shoulder and the D-ring (Shoulder), lower shoulder-belt before the buckle (Lap), and at the outboard end of the belt before the anchoring point to the sled buck (Side). For each configuration result time history corridors, consisting of upper and lower bounds of the PMHS landmark displacements, lateral lean, torso twist and belt forces, were created using time and excursion standard deviations from the PMHS tested in the corresponding configuration (Appendix A), except for configurations 4 and 6, where only one subject was tested. For these two test configurations, corridors were created by using the standard deviation from PMHS tested in similar test conditions (Appendix A). For each test configuration, a total of 20 response corridors were created (Table II).

TABLE II
MEASUREMENTS USED FOR CREATING PMHS CORRIDORS FOR EACH TEST CONFIGURATION.

Measurement	Comp 1	Comp 2	Comp 3	Unit
Head displacement	X	Y	Z	mm
Left Acromion displacement	X	Y	Z	mm
Right Acromion displacement	X	Y	Z	mm
T1 displacement	X	Y	Z	mm
Pelvis displacement	X	Y	Z	mm
Belt Forces	Shoulder	Lap	Side	N
Thorax	Lateral Lean	Torso Twist	-	Degrees

In the development of countermeasures, it is necessary to consider robustness of the restraint system by addressing variations in uncontrollable factors, such as occupant position, impact directions and presence of another occupant in the same seating row. Therefore, validated computational HBMs complement crash test dummies and crash test dummy models for evaluations of occupant loading with varying obliquity. In the future, validated HBMs can be used to complement consumer rating with respect to robustness.

The aim of the study is to confirm the capability of a modified version of the HBM THUMS V3 to predict human kinematics and the risk to sustain rib fractures in far-side impacts, and thereafter to use the model to demonstrate the potential injury-reducing benefits and range of protection of a far-side impact protection system. An extended aim is to evaluate the performance of the protection system in the proposed Euro-NCAP 2020 far-side impact test protocol.

II. METHODS

THUMS Far-side Biofidelity Evaluation

For this study a modified version of THUMS v3 [11] was used. Modifications included remodeling of the ribcage [12] and recalibration of the lumbar spine properties [13] (modifications are listed in Appendix F). The ribs are modeled by means of homogeneous isotropic, linear elastic-plastic materials. The trabecular and cortical bone are modelled by means of solid and shell elements respectively. The costal cartilage and the ligaments are modelled by means of homogeneous, isotropic linear elastic materials. The risk of rib fracture is assessed by means of a probabilistic method [9]. In the method the element with highest peak 1:st principal strain in the cortical bone of each rib is used to assess the rib fracture risk. Element deletion is not used.

The biofidelity evaluation for far-side loading of the modified THUMS model was carried out by means of the PMHS tests conducted by Forman *et al.* [10] and the biofidelity corridors calculated according to method in Appendix A. In addition to the kinematic evaluation, the model was also evaluated for the ability to predict rib fractures.

The modified THUMS model was positioned in a model of the test buck, in the average measured position of all PMHS used in the test configurations [10] and settled by gravity load. The seat-belt model D-ring, buckle and outboard anchoring positions were also adjusted relative to the left acromion and midpoint of left and right Posterior Superior Iliac Spine (PSIS) on the positioned THUMS model, to keep the same angle in the sagittal plane between D-ring and left acromion and between buckle and anchor to PSIS to that of the average PMHS tested in the configuration. Initial position of THUMS and of the three PMHS tested in configuration 2 is shown in Fig. 1.

The THUMS-to-seatbelt and THUMS-to-test buck contact friction coefficients were defined using a parameter identification method. Predicted shoulder-belt force and pelvis lateral (Y) displacement time histories for configuration 3 (Table I) were matched to the mean results from the three PMHS sled tests in the same configuration. The resulting coefficient was 0.7 for both contacts.

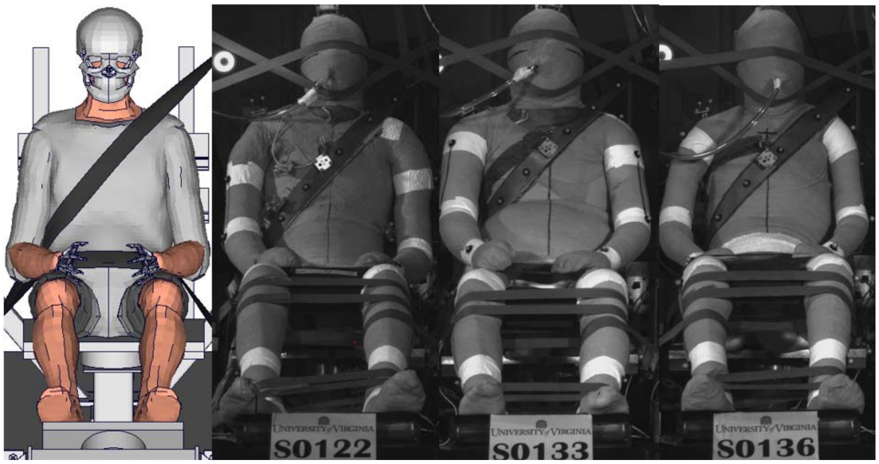

Fig. 1. Initial position of THUMS and of the three PMHS tested in configuration 2.

The test buck FE-model was impacted with a ΔV of 16 km/h or 34 km/h. The pulse was obtained from the PMHS testing in the impact direction of the relevant configuration. A visual comparison between the predicted kinematics and the PMHS kinematics and a CORA evaluation were carried out.

Time histories for the 20 measurements (Table II) were extracted from the simulations and a CORA [14] rating analysis (corridor method using PMHS corridors as inner bounds + cross correlation method on the mean trace of PMHS corridor upper and lower bound) was carried out for each measurement (Appendix B). The CORA rating for a signal ranges from 0 to 1, where 0 means no correlation and 1 is perfect correlation. For each configuration the CORA rating was calculated as the mean of the 20 individual measurement ratings, and the THUMS overall CORA rating was calculated as the mean of the six resulting configuration CORA ratings. For an overall CORA rating above 0.65 the model was considered valid. This value is adapted from the ISO/TR 9790 [15] biofidelity rating scale for side-impact dummies (rating 0–10), where a Good biofidelity classification is achieved for a rating ≥6.5/10. The 0.65 rating level was assumed also to be applicable for human body models. The probabilistic rib fracture risk prediction method developed by Forman *et al.* [9], based on the predicted maximum principal strain in the rib cortical bone, was used to predict the risk for a 65 year old occupant to sustain 2 or more fractured ribs. All simulations were performed using LS-Dyna mpp s R7.1.2 rev 95028 (LSTC).

Injury-reducing Benefits of a Far-Side Airbag

A simplified sled model, based on the mid-size sedan vehicle used for this study, was created according to the proposed Euro-NCAP specification [6. The sled model comprised driver and passenger seat, the center console, the doors and rigid BIW (Fig. 2). The modified THUMS model was positioned in the driver seat and belted with a retractor pre-tensioning 3-point seat-belt system model. The crash pulses used to accelerate the sled model were non-struck B-pillar pulses recorded in 60 km/h 1400 kg AE-MDB-to-car and 32 km/h 75° car-to-rigid-pole tests performed with the vehicle. The pulses were scaled and applied in a 75° far-side direction, according to the assessment protocol [6]. Sled test simulations were performed, and predicted lateral head excursion and rib fracture risk were evaluated. The lateral head excursion was measured as the maximum lateral distance from the undeformed driver seat centreline to the most inboard point of the head during the crash event, measured relative to the moving BIW. Based on in-house measurements, the friction coefficient used was 0.3.

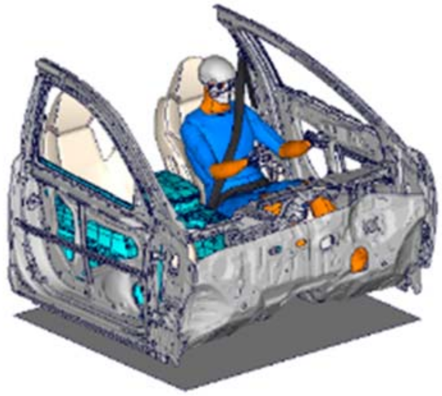

Fig. 2. Sled model for far-side sled test evaluation, including belted occupant, centre console, seats, doors and rigid BIW.

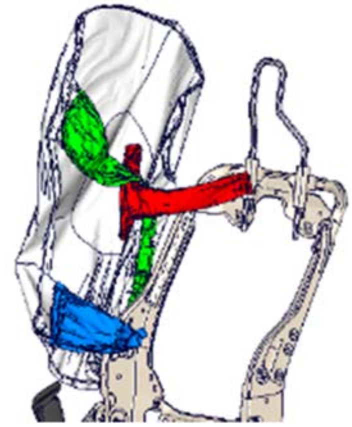

Fig. 3. Far-side airbag model mounted to seat frame.

The injury-reducing benefit of a seat-mounted far-side airbag was evaluated. The airbag model was attached to the frame of the driver seat. Three tethers were also attached to the seat frame (Fig. 3). The airbag model was inflated from an unfolded configuration (Fig. 3). The inflated volume of the airbag was 22 litres and the pressure was 90 kPa. The airbag model uses validated material models, and the system model (gas inflator and current geometry) was correlated to test data from a static deployment test (Appendix B).

Range of Protection Evaluation of the Far-Side Airbag

The range of protection of the far-side airbag was evaluated by means of 60 km/h, 1400 kg AE-MDB model (version 1.0.070613, 100 kg mass added to trolley, LSTC) to vehicle simulations. The vehicle model was impacted at 90°–15° in 15° intervals, with the AE-MDB model centreline aimed at the impact location used in the AE-MDB-to-vehicle side-impact testing, but mirrored to the far-side from the driver (Fig. 4.) The THUMS model was positioned in the driver seat of the vehicle and belted with the same pre-tensioning 3-point belt system model that was used in the sled simulations. Simulations with and without the far-side airbag were carried out. Lateral head excursion was measured relative to the non-struck B-pillar and the risk for a 65 year old occupant to sustain 2 or more fractured ribs was evaluated.

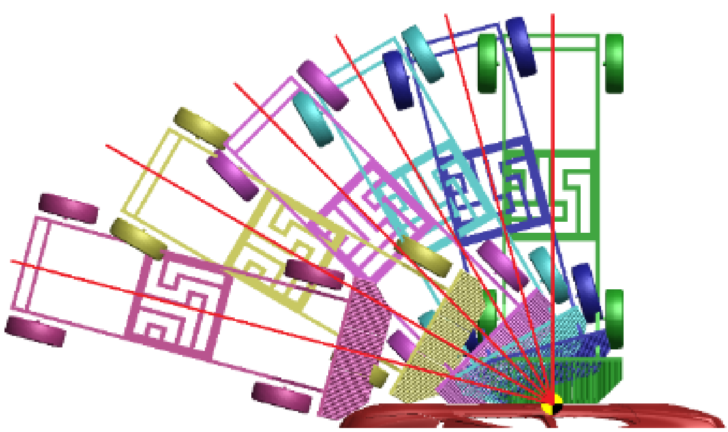

Fig. 4. Overview of initial direction and position of the AE-MDB model for the AE-MDB-to-vehicle simulations.

Euro-NCAP Far-Side Sled Test Rating Evaluation

The WorldSID 50%-ile male FE-model (PDB WorldSID RHD model v4.0.3 Dynamore GmbH, Stuttgart, Germany) was positioned and belted in the sled model. Euro-NCAP AE-MDB and rigid pole sled test simulations were performed with and without far-side airbag. Predicted lateral head excursion, upper neck forces and moments, chest compression, abdomen compression, pubic forces and lumbar forces and moments were evaluated by means of the proposed Euro-NCAP limits [6]. The occupant to occupant interaction limit for the studied vehicle was located 520 mm inboard from the driver seat centerline.

III. RESULTS

THUMS Far-side Biofidelity Evaluation

The general validation of the model was assessed using CORA. However, the interaction between the belt and the upper body was assessed by means of visual comparison between the predictions from the model and results from the PMHS tests. Generally, the interaction between the belt and the upper body of the PMHS was predicted with the model. However, in some repeated PMHS tests there were some differences in the sliding of the belt along the chest between the different PMHS. In configuration 3, the belt slipped off the shoulder of one PMHS, while it stayed on the shoulder for the other two PMHS (Fig. 5). In the model, the belt remained on the shoulder for the duration of the test.

Fig. 5. Snapshots at 140 ms. Test configuration 3. THUMS model in the sled buck model, and the three PMHS tests in this configuration: S0123, S0134 and S0137.

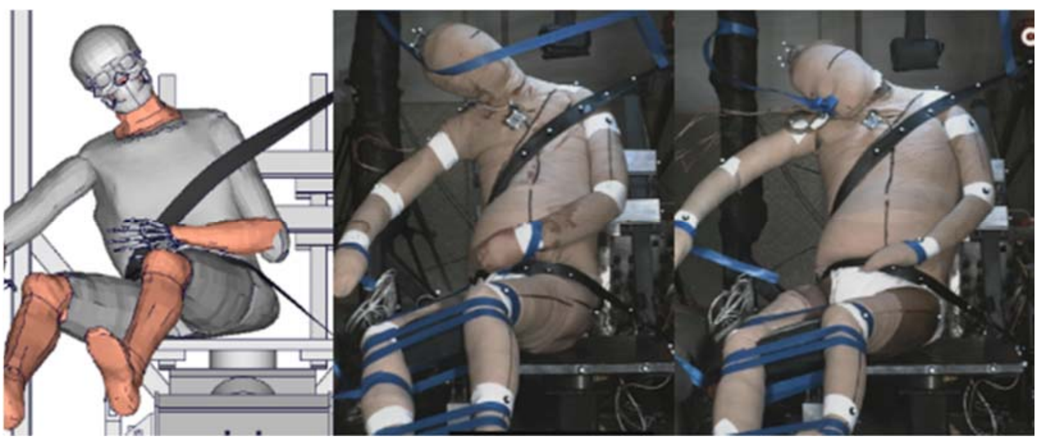

Fig. 6. Snapshot at 140 ms. THUMS and the two PMHS tests in configuration 5: S0083 and S0088.

In configuration 5, the belt stayed on the shoulder of both PMHS (Fig. 6). In the model, however, the belt slipped off the shoulder. (Images from all configurations can be found in Appendix 0.)

The resulting overall CORA rating for all configurations was 0.76, with a median value of 0.78 (Table III). The lowest rating was 0.60, which was in configuration 5 (low speed 90°), and the highest rating was 0.87, which was in configuration 2 (low speed 60°, no pre-tensioning). Plots of all PMHS corridors, THUMS predictions and individual measurement CORA results can be found in Appendix D.

TABLE III

BIOFIDELITY EVALUATION CORA ANALYSIS RESULTS

Configuration:	***1***	***2***	***3***	***4***	***5***	***6***	***Overall***
CORA Rating:	0.79	0.87	0.69	0.78	0.60	0.83	0.76

The predicted rib fracture risk was 0% for 2+ fractured ribs for a 65yo occupant in all low-speed impact configurations (ΔV=16 km/h no. 2, 3, 4 and 5). In the high-speed impact configuration (high speed, ΔV=34 km/h), the predicted risk for 2+ fractured ribs for a 65yo occupant was 98% in configuration 1 and 95% in configuration 6. Total number of PMHS rib fractures identified after testing was 16 (PMHS 591), and 10 (PMHS 602) in configuration 1, and 24 (PMHS 559) in configuration 6 [10]. In all low-speed PMHS tests there were no fractures in the PMHS and the model predicted no rib fractures. In all high-speed PMHS tests there were more than two rib fractures in all PMHS and there was a 98% and a 95% predicted risk of 2+ fractured ribs.

Injury-reducing Benefits of a Far-Side Airbag

The predicted head excursion in the AE-MDB sled configuration was 648 mm and in the rigid pole configuration was 659 mm (Table IV). With the addition of a far-side airbag, head excursion was reduced to 506 mm in the AE-MDB sled configuration and to 486 mm in the rigid pole configuration.

TABLE IV

LATERAL HEAD EXCURSION IN THUMS FAR-SIDE SLED TEST SIMULATIONS

Far-side Airbag	**AE-MDB (mm)**	**Rigid Pole (mm)**
No	648	659
Yes	506	486

The predicted risk of more than 2 fractured ribs was reduced to 0% from 91% for a 65yo occupant in the AE-MDB, and from 46% in the Pole impact sled simulations when the far-side airbag was introduced (Table V).

TABLE V

THUMS PREDICTED RISK OF 2 OR MORE FRACTURED RIBS 65YO OCCUPANT,

WITH AND WITHOUT FAR-SIDE AIRBAG

Far-Side Airbag	***AE-MDB***	***Rigid Pole***
No	91%	46%
Yes	0%	0%

Range of Protection Evaluation of the Far-Side Airbag

Head lateral excursion was reduced from 719 mm to 371 mm as the impact angle was reduced from 90° to 15° (Table VI). The addition of a far-side airbag reduced head lateral excursion from 719 mm to 516 mm for the 90° AE-MDB impact, and from 371 mm to 253 mm for the 15° impact.

TABLE VI

THUMS-PREDICTED MAXIMUM LATERAL HEAD EXCURSION IN AE-MDB-TO-VEHICLE SIMULATIONS

AE-MDB Direction	*90°*	*75°*	*60°*	*45°*	*30°*	*15°*
No Airbag (mm)	719	673	614	528	456	371
Far-side Airbag (mm)	516	448	428	342	320	253

Predicted risk for 2+ fractured ribs were 96%, 78% and 75% for 90°, 75° and 60° AE-MDB impacts respectively and 0% in the 45° and 30° impacts. For 15° there was a 100% predicted risk for 2+ fractured ribs (Table VII). With the addition of a far-side airbag, the risk was reduced to 1% in the 90° AE-MDB impact, and to 0% for the 75°–30° impact. In the 15° impact with the far-side airbag there was a 1% risk for 2+ fractured ribs. (See Appendix E for the maximum principal strain in each rib cortical bone used for rib fracture risk calculation in the robustness simulations.)

TABLE VII

THUMS-PREDICTED RISK OF TWO OR MORE RIBS FRACTURED IN AE-MDB-TO-VEHICLE SIMULATIONS

AE-MDB Direction	***90°***	***75°***	***60°***	***45°***	***30°***	***15°***
No Airbag	*96%*	78%	75%	0%	0%	100%
Far-side Airbag	*1%*	0%	0%	0%	0%	1%

Euro-NCAP Far-Side Sled Test Rating Evaluation

In the Euro-NCAP far-side sled test simulations the predicted WorldSID head lateral excursion was 644 mm and 692 mm for the AE-MDB and pole configurations, respectively. The occupant interaction limit (520 mm lateral excursion) was exceeded for both configurations. When the far-side airbag was included, the WorldSID predicted head excursion was 512 mm and 491 mm for AE-MDB and pole configurations, respectively. That was less than the occupant interaction limit for both configurations (Fig. 7 and Fig. 8). In all simulations, with and without far-side airbag, the predicted WorldSID head lateral excursion was less than the higher performance limit (yellow line) and the maximum intrusion limit (red line) of the vehicle.

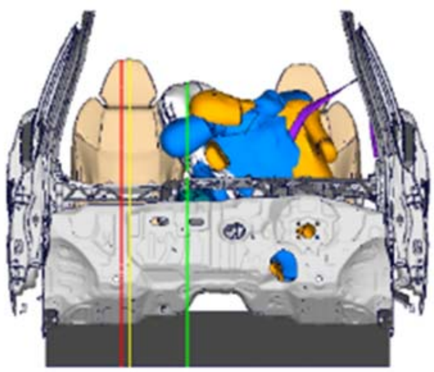

Fig. 7. WorldSID maximum head excursion in AE-MDB sled test simulation (blue is WorldSID without far-side airbag).

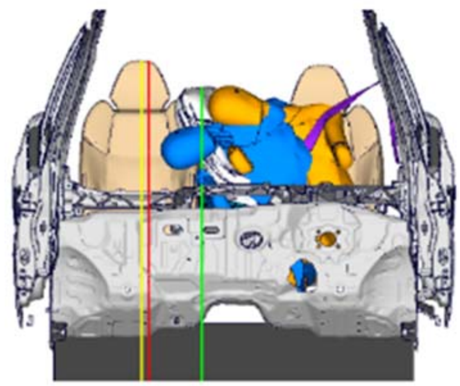

Fig. 8. WorldSID at maximum lateral head excursion in the Pole impact sled test simulation (blue is WorldSID without far-side airbag).

Predicted WorldSID injury criteria, together with the Euro-NCAP scoring limits [6], are presented in Table VIII (values in brackets are under examination by Euro-NCAP and are not included in the rating, but can be included at a later date). In both cases, all predicted WorldSID injury criteria values were reduced when the far-side airbag was added, and were lower than the defined high-performance limits and monitored limits. Without far-side airbag, the high-performance chest compression limit was exceeded in the pole impact configuration.

TABLE VIII
WORLDSID INJURY CRITERIA EXTRACTED FROM SLED TEST SIMULATIONS AND EURO-NCAP CRITERIA LIMITS

WorldSID Criteria	***AE-MDB***		***Pole impact***		***Euro-NCAP***		
	No Airbag	***Far-Side Airbag***	***No Airbag***	***Far-Side Airbag***	***Hi. Perf.***	***Lo. Perf.***	***Capping***
HIC_{15}	131	64	85	31	500	700	700
Head acc.3ms	41	30	34	21	72 g	80 g	80 g
Upper Neck F_z	1.52	0.93	1.29	0.58	-	3.74 kN	-
M_x	45	22	25	21	-	[50 Nm]	-
M_y	34	18	28	13	-	[50 Nm]	-
Chest comp.	14	13	40	12	28 mm	50 mm	50 mm
Abd. Comp.	23	19	18	16	[47 mm]	[65 mm]	[65 mm]
Pubic F_y	0.8	0.6	0.5	0.4	-	2.8 kN	-
Lumbar F_y	1.2	0.6	0.8	0.2	-	[2.0 kN]	-
F_z	2.72	1.6	2.41	1.5	-	[2.84 kN]	-
M_x	80	64	66	19	-	[100 Nm]	-

IV. DISCUSSION

In the visual comparison some variability in the shoulder-belt and chest interaction in the PMHS tests was observed. The anthropometry of the PMHS can influence the sliding of the shoulder-belt over the chest of the occupant. The THUMS model can be considered to correspond to one individual. Therefore, to mimic PMHS shoulder-belt and chest interaction of various PMHS, there is a need to morph the HBM to the anthropometry of that specific PMHS.

The kinematics of the legs and feet was observed to differ between THUMS and PMHS. One reason was that the kinematics of the legs of the PMHS was influenced by foam blocks that were positioned between the legs. In addition, tape was wrapped around the legs. The foam block and tape were not included in the model due to the fact that in a passenger vehicle, the motion of the legs and feet are limited by the vehicle interior. In addition, modelling the foam block and tape was not considered since the documentation was not at a level of detail necessary for modelling. Therefore, no correlation analysis was carried out for the kinematics of the THUMS lower extremities.

In a study by Katagiri *et al.* [16], the biofidelity of a modified GHBMC AM50-O v4.4 HBM was assessed using PMHS tests carried out by Forman *et al*. [10]. The HBM was positioned according to a specific PMHS for each simulation. The shoulder-belt to HBM friction coefficient was adjusted based on the impact direction, and the biofidelity was assessed by visual comparison of the time history curves. The limitations with the approach used by Katagiri *et al*. are that the biofidelity judgement is not objective and the ability of the model to predict PMHS response under other circumstances is limited.

Over all configurations, the THUMS model obtained a CORA rating of 0.76 when evaluated for correlation with the PMHS corridors. The lowest configuration rating was 0.60, obtained in configuration 5, where the THUMS model slipped out of the shoulder-belt more than for the two PMHS and thus produced a different kinematic response. This indicates that a CORA rating of 0.65 or above can serve as a limit of acceptable correlation in this investigation. The CORA score is a general estimate of the biofidelity of the model. For the far-side assessment carried out the predicted head excursion was considered important. In addition, the CORA score was complemented with a comparison between the predicted belt chest interaction and the belt chest interaction in the PMHS tests. In addition, the chosen lower limit of a total CORA rating 0.65 is arbitrarily set, and might need reconsideration, especially if more PMHS data is obtained, or if individual measurement weights are adjusted.

The predicted rib fracture risk was high in the high-speed configurations, and low for all the low-speed configurations. Since all PMHS tested in the high-speed configurations were subjected to previous testing in low-speed configurations and palpation was used to investigate thoracic injuries after the low-speed tests, fractures could have been sustained in the low-speed tests. However, the large number of fractures obtained in each PMHS after high-speed testing implies that the high-speed case alone was injurious. Due to the fact that the model predicted high risk of 2+ fractured ribs and the PMHS sustained a great number of rib fractures the rib fracture prediction method was considered valid. In addition, since element deletion is not used the added load on remaining non-fractured ribs when a rib fractures is not accounted for. Therefore, the method is used to assess a limited number of fractured ribs.

The PMHS tests that were used in the biofidelity evaluation were carried out in a generic sled test buck. The buck consisted of a simplified rigid seat, footrest, and in one configuration a plate blocking the lateral motion of the pelvis. The Euro-NCAP sled test configuration consisted of deformable seats, centre console, and footwell and seat-belt attachment points controlled by the vehicle design. For the biofidelity evaluation there were some important similarities between the two configurations when no far-side airbag was present. In both the PMHS test configuration and the Euro-NCAP configuration the major part of the load on the body was from the seat-belt and the centre console. The Euro-NCAP impact direction was set to 75°, which is in the middle of the 90° and 60° directions used in the PMHS sled tests. The ΔV of the vehicle pulses was 31 km/h for the AE-MDB and 38 km/h for the rigid pole, which is comparable to the ΔV=34 km/h high-speed pulse in the PMHS testing.

For the THUMS Euro-NCAP sled test evaluations the lateral head excursion was greater and the predicted risk of rib fractures was lower in the pole impact configuration than for the AE-MDB configuration. This difference was due to the different characteristics of the applied sled test pulses. The AE-MDB pulse was a high acceleration and short duration pulse, while the pole impact pulse was low acceleration and long duration. Although lower in magnitude, the long duration of the acceleration pushed the occupant’s upper body further out of position after slipping out of the shoulder-belt than in the AE-MDB case. Including the far-side airbag reduced risk of injury by protecting the ribs from the vehicle interior and reducing head excursion and thus the risk of the head impacting the struck side intruding door or a near-side seated occupant.

The range of protection evaluation of the far-side airbag showed the capability of a far-side airbag to reduce head excursion and risk of rib fractures in far-side impacts beyond the simplified sled testing. In this study, however, it was limited only to simulations with different impact directions of the AE-MDB. Varying parameters, such as load case, seat position, occupant size and seating position, may be considered in future work.

When the far-side airbag was used in the Euro-NCAP far-side sled test rating evaluation with the WorldSID, a full rating score was obtained. Without the far-side airbag, score reductions were obtained by exceeding the occupant interaction limit (negative modifier reduces total score from each test by 50%) in both cases. In the Pole impact simulation, the score was further reduced by exceeding the high-performance limit for chest compression. Based on the kinematics, it is also assumed that the far-side airbag would prevent head-to-head contact in case of an adjacent occupant, as was also shown by [5].

The Pole impact configuration resulted in greater predicted chest compression in the lowest thoracic rib IR-TRACC than what was obtained in the AE-MDB configuration. The low acceleration in the Pole impact configuration resulted in the WorldSID being pushed further down into the seat than in the AE-MDB configuration before contacting the centre console, due to the force from the pre-tensioning of the lap belt. When contact between the WorldSID torso and centre console was initiated in the Pole configuration, the upper corner of the centre console loaded the third thoracic rib. In the AE-MDB configuration the load from the centre console was distributed between the abdominal and third thoracic ribs. The discrete, horizontal rib design of the WorldSID was sensitive to the loading pattern and could predict high injury risk in load cases where a HBM predicts low injury risk, and vice versa. A centre console can be designed such that the WorldSID third thoracic rib will always strike above the centre console in a far-side impact, and thus predict a low thoracic injury risk, while a HBM may predict a high risk for a chest injury.

V. CONCLUSIONS

1. The modified THUMS model can be used to evaluate head excursion and rib fracture risk in far-side loading.
2. The proposed far-side airbag reduces head excursion and risk of chest injury.
3. The proposed far-side airbag reduced head excursion in far-side impact from 90° to 15° impact.
4. The studied vehicle fulfilled the Euro-NCAP 2020 far-side impact sled test requirements when using the proposed far-side airbag.

VI. REFERENCES

[1] Gabler, C., *et al*. (2005) Far Side Injury Risk for Belted in Australia and the United States. *Proceedings of the ESV Conference, 2005, Washington D. C., USA.*

[2] Yoganandan, N., *et al*. (2014) Crash Characteristics and Injury Patterns of Restrained Front Seat Occupants in Far-side Impacts. *Traffic Injury Prevention*, *2014, 15: pp. S27–S34.*

[3] Fildes, B., Vulcan, P., Lane, J. and Lenard, A. (1995) Side impact crashes in Australia. *Proceedings of the International Technical Conference on the Enhanced Safety of Vehicles*, 1995, Munich, Germany.

[4] Bostrom O, Gabler HC, Digges K, Fildes B, Sunnevang C. Injury Reduction Opportunities of Far side Impact Countermeasures. *Annals of Advances in Automotive Medicine / Annual Scientific Conference. 2008, 52: pp.289-300, San-Diego.*

[5] Newland, C., *et al*. (2008) Occupant-to-Occupant Interaction and Impact Injury Risk in Side Impact Crashes. *Stapp Car Crash Journal,* 2008, 52: pp. 327-47.

[6] European New Car Assessment Programme (2017). Far Side Occupant Test & Assessment Procedure Version 1.0.

[7] Pintar, F., *et al.* (2007) Comparison of PMHS, WorldSID, and THOR-NT Responses in Simulated Far Side Impact. *Stapp Car Crash Journal, 2007, 51: pp. 313-60.*

[8] Nahum, A., Melvin, J. (1993) Accidental Injury Biomechanics and Prevention, Second Edition, pp 161-164, Springer-Verlag, New York, USA, 1993.

[9] Forman, J., *et al.* (2012) Predicting Rib Fracture Risk with Whole-Body Finite Element Models: Development and Preliminary Evaluation of a Probabilistic Analytical Framework. *Proceedings of the 56th AAAM Annual Conference on Annals of Advances in Automotive Medicine, 2012, 56: pp. 102–24.*

[10] Forman, J., *et al*. (2013) Occupant Kinematics and Shoulder Belt Retention in Far-Side Lateral and Oblique Collisions: A Parametric Study. *Stapp Car Crash Journal, 2013, 57: pp. 343-85.*

[11] Iwamoto, M., Kisanuki, Y., Watanabe, I., Furusy, K., Miki, K. (2002) Development of a Finite Element Model of the Total Human Model for Safety (THUMS) and Application to Injury Reconstruction. *Proceedings of the IRCOBI Conference, 2002, Munich, Germany.*

[12] Iraeus, J., Davidsson, J., Brolin, K. (2017) Recent HBM activities at Chalmers University. *International VDI conference*, *2017, Berlin, Germany.*

[13] Afwerki, H. (2016) Biofidelity Evaluation of Thoracolumbar Spine Model in THUMS. Master's Thesis in Biomedical Engineering, *Chalmers University of Technology, 2016, Gothenburg, Sweden.*

[14] Gehre, C., Gades, C., Wernicke, P. (2009) Objective Rating of Signals Using Test and Simulation Responses. *Proceedings of the 21st ESV conference, 2009, Stuttgart, Germany.*

[15] International Organization for Standardization (1999) Technical Report 9790; Road Vehicles; Anthropomorphic side impact dummy - lateral impact response requirements to assess the biofidelity of the dummy. IOS, Geneva.

[16] Katagiri, M., Zhao, J., Kerrigan, J., Kent, R., Forman, J. (2016) Comparison of Whole-Body Kinematic Behavior of the GHBMC Occupant Model. *Proceedings of the IRCOBI Conference, 2016, Malaga, Spain.*

VII. APPENDIX

A. PMHS corridor calculation method

Introduction

This method elaborates previous techniques by Lessley *et al*. [A1] and Shaw *et al*. [A2]. The main characteristic of these techniques is the parametrisation of the response. This approach is adopted to better account for possible differences in time-to-peak in the individual responses.

Corridor Calculation

First, parametrise each curve by its arc-length, with the arc-length along the curve normalised based on the arc-length between two characteristic points on the curve (from the value at time 0 ms to the peak value, Fig. A-1, a and b). Second, calculate the mean and standard deviation in each axis (e.g. time and displacement) for each step in arc-length (Fig. A-1, c and d). Third, define the corridor as the set of ellipses with centres at each step in arc-length along the mean curve and semi-axes proportional to the standard deviation in each axis at each step in arc-length (Fig. A-1, e and f).

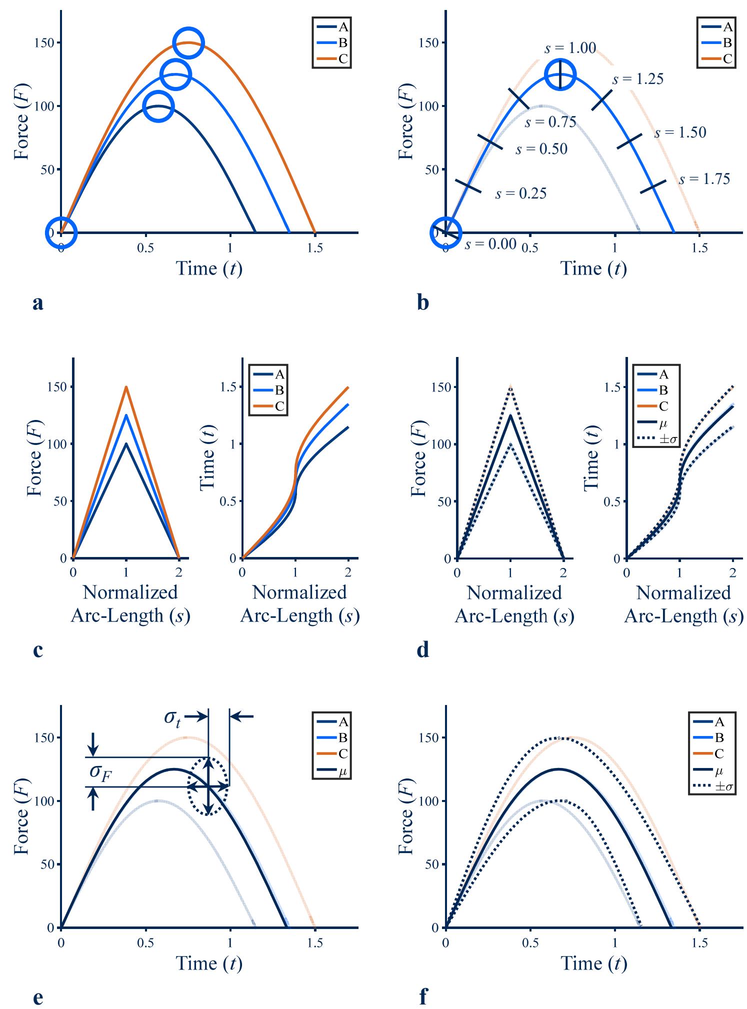

Fig. A-1. Illustration of parametrisation (a, b, c) and corridor creation (d, e, f) for an example data set (individual force time-histories A, B and C). The mean (μ) and standard deviation (σ) were calculated for force (F) and time (t) separately as functions of normalised arc-length (s).

Corridor Calculation Method for Single-Sample Tests

For a given test condition (*A*) with n>1 cadavers, we can create a *confidence interval* (corridor) using the mean and some multiple of the standard error (SE_A) of the individual responses. We can also calculate the sample standard deviation (s) of the individual responses, where $SE_A = s/\sqrt{n}$.

For a similar test condition (*B*) with n=1 cadaver (whether or not that same cadaver was tested in test condition (*A*)), we can create a *confidence interval* (corridor) using the cadaver's response and some multiple of the square root of the sum of the squared standard error and squared sample standard deviation from test condition (*A*), i.e. $SE_B = \sqrt{s^2 + SE_A^2} = \sqrt{s^2 + s^2/n} = s\sqrt{1 + 1/n}$.

For the present study, the n>1 and n=1 tests (with associated most similar tests) are listed in TABLE A I and TABLE A-II. Most similar test conditions to the n=1 tests were selected based on available n>1 tests and identical parameters (e.g. acceleration, principal degree of force) in as many ways as possible and ordered according to the sensitivity analysis of Forman *et al*. (2013) [A3].

TABLE A I

TESTS UTILIZED IN CORRIDOR GENERATION (N>1)

Condition Code*	Tests
14/O/T/I/Yes/No	S0124, S0135
6.6/O/T/I/No/No	S0122, S0133, S0136
6.6/O/T/I/Yes/No	S0123, S0134, S0137
6.6/L/T/F/Yes/No	S0083, S0088
6.6/O/T/B/Yes/No	S0127, S0132, S0139

TABLE A-II

TESTS UTILIZED IN CORRIDOR GENERATION (N=1)

Condition Code*	Test	Closest Condition	Closest Tests
6.6/O/T/B/Yes/Yes	S0129	6.6/O/T/B/Yes/No	S0127, S0132, S0139
14/L/T/I/Yes/No	S0091	6.6/L/T/F/Yes/No	S0083, S0088

*Condition code: Pulse (g) / Direction / Arm Position / D-Ring Position / Pretensioner / Pelvis Block
Direction: L=Lateral, O=Oblique; Arm Position: T=On Thighs, K=On Knees, U=Up
D-Ring Position: B=Back, I=Intermediate, F=Forward

References

[A1] Lessley D, Crandall J, Shaw G, Kent R, Funk J. (2004) A normalization technique for developing corridors from individual subject responses, *SAE Technical paper, 2004-01-0288, 2004.*

[A2] Shaw JM, Herriott RG, McFadden JD, Donnelly BR, Bolte JH. (2006) Oblique and lateral impact response of the PMHS thorax, Stapp Car Crash Journal, 2006,50: pp.146-67.

[A3] Forman, J., et al. (2013) Occupant Kinematics and Shoulder Belt Retention in Far-Side Lateral and Oblique Collisions: A Parametric Study. *Stapp Car Crash Journal, 2013, 57: pp. 343-85.*

B. Far-side Airbag static deployment test and simulation

Pictures from far-side airbag static deployment test and simulation of the test with the far-side airbag model are presented in Fig. B.1 and Fig. B.2 with side and frontal views respectively. Measured airbag pressure from the test and resulting pressure in the simulation of the test is presented in Fig. B.3.

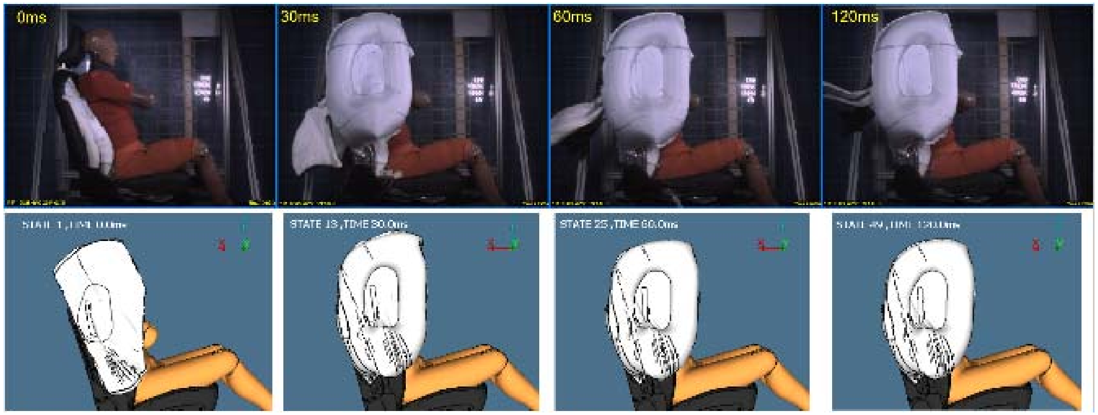

Fig. B.1. Top: Side view of far-side airbag static deployment test. Bottom: Side view of static deployment simulation. Airbag model inflated from unfolded configuration.

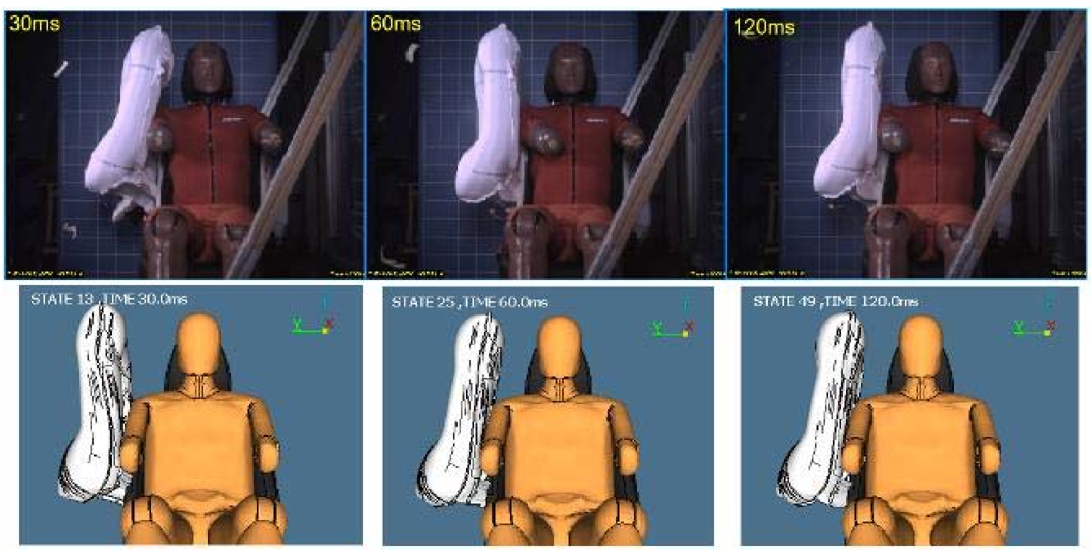

Fig. B.2. Top: Front view of far-side airbag static deployment test. Bottom: Front view of static deployment simulation.

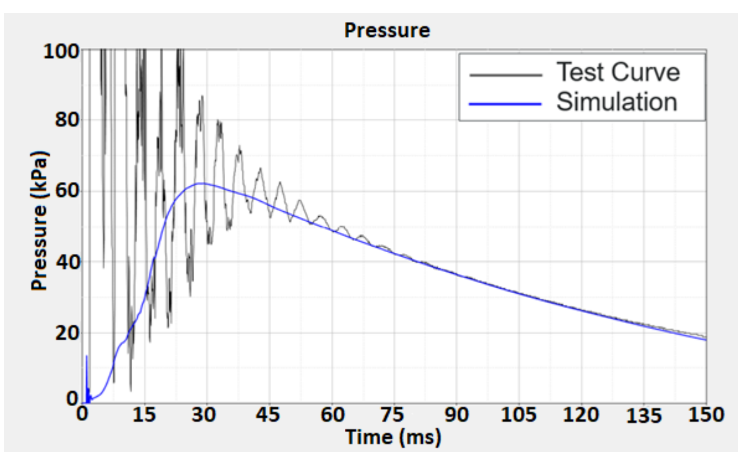

Fig. B.3. Far-side airbag pressure from static deployment test and the static deployment test simulation.

C. Visual comparison of THUMS and PMHS Kinematics

Pictures of THUMS simulation and the PMHS tested in the same configuration is presented here in Fig. C.1–Fig. C.6.

Fig. C.1. Snapshot at 120 ms. THUMS and the two PMHS tested in configuration 1.

Fig. C.2. Snapshot at 140 ms. THUMS and the three PMHS tested in configuration 2.

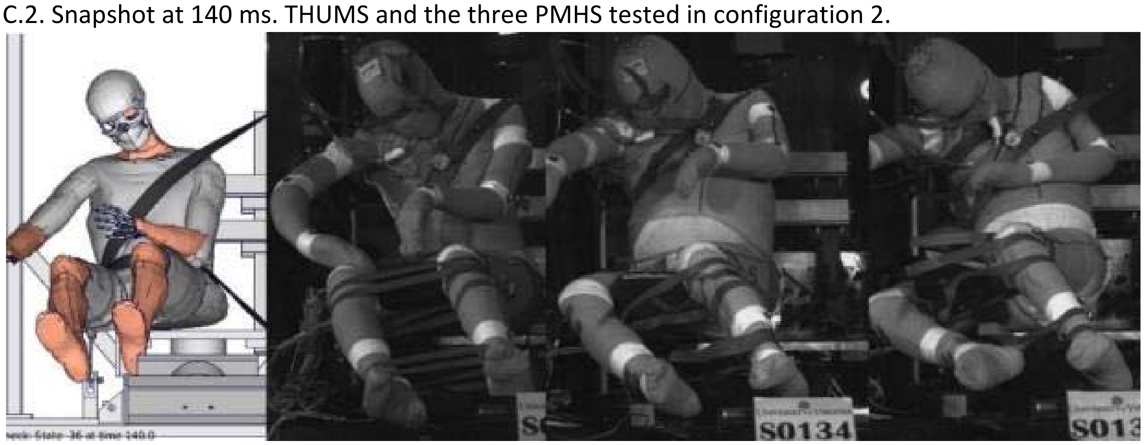

Fig. C.3. Snapshot at 140 ms. THUMS and the three PMHS tested in configuration 3.

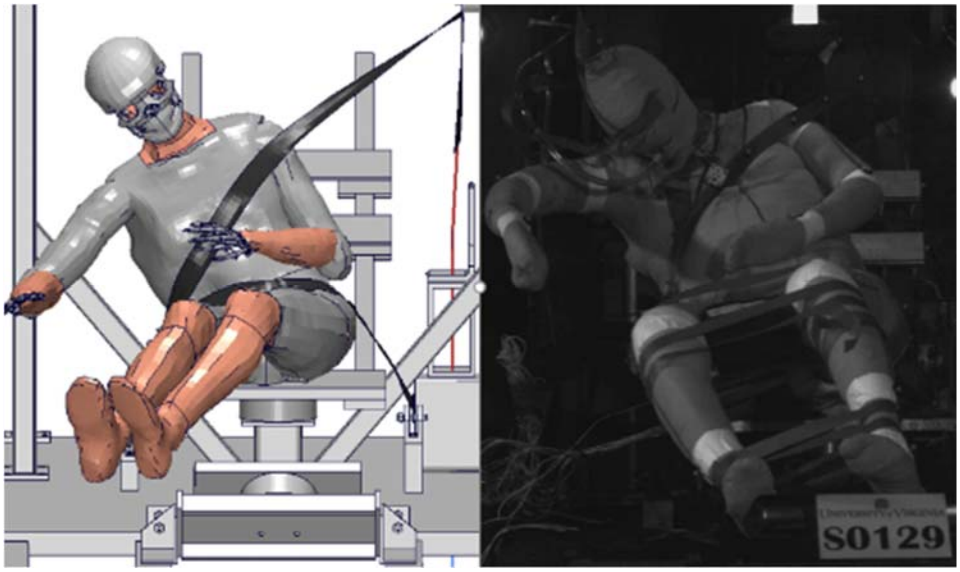

Fig. C.4. Snapshot at 140 ms. THUMS and the PMHS tested in configuration 4. PMHS has foam blocks between knees and feet.

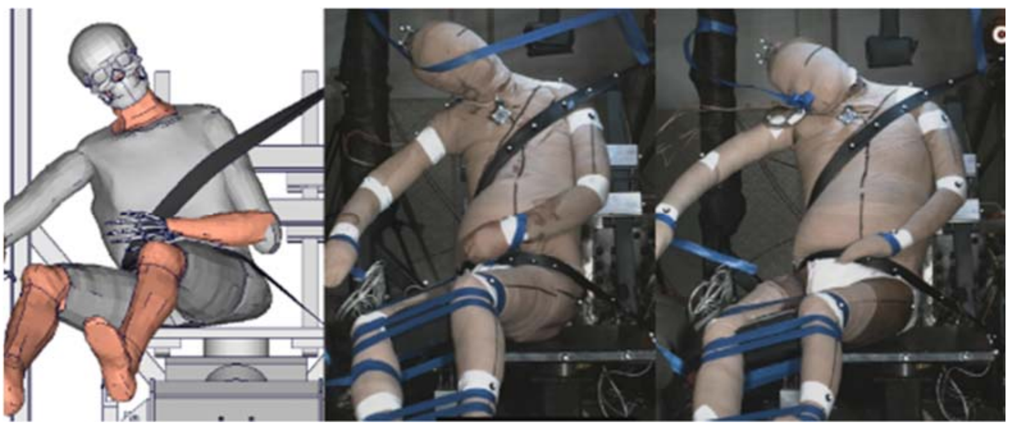

Fig. C.5. Snapshot at 140 ms. THUMS and the two PMHS tested in configuration 5.

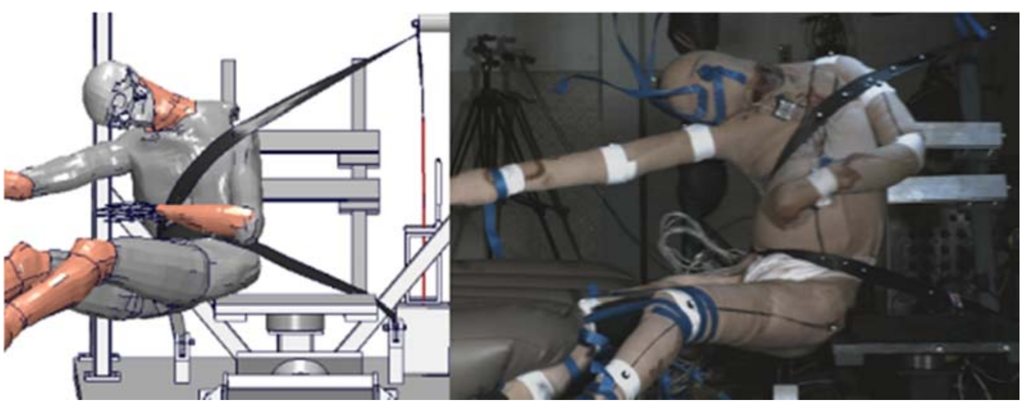

Fig. C.6. Snapshot at 140 ms. THUMS and the PMHS tested in configuration 6. The gap between left upper arm and shoulder in the THUMS model is a result of disjoint meshes between torso and arm soft tissues in the THUMS v3 baseline model, leading to the belt pressure compressing only the upper arm mesh once the shoulder has slipped out of the belt.

D. CORA evaluation parameter settings, THUMS Predictions and PMHS Corridors with CORA Rating

The settings used for all individual signal ratings in the CORA evaluation are presented in Table D.I. Simulation results, together with PMHS corridors and individual CORA rating for each signal from the six simulated configurations, are presented in Fig. D.1-Fig. D.18.

TABLE D.I
CORA PARAMETER SETTINGS USED FOR ALL CORA RATINGS

	Parameter	***Setting***	***Explanation***
Time Interval Settings	A_THRES	0.03	Threshold to set the start of the interval of evaluation
	B_THRES	0.075	Threshold to set the end of the interval of evaluation
	A_EVAL	0.01	Extension of the interval of evaluation
	B_DELTA_END	0.001	Additional parameter to shorten the interval of evaluation
	T_MIN/ T_MAX	auto/auto	Start time and end time of the interval of evaluation (automatic = calculated for each channel)
Corridor Method	K	2	Transition between ratings of 1 and 0 of the corridor method
	G_1	0.5	Weighting factor of the corridor method
	a_0/b_0	0.05/ 0.50	Width of the inner and outer corridors
	a_sigma/ b_sigma	1/1	Multiples of the standard deviation to widen the inner and outer corridors
Cross-Correlation Method	D_MIN	0.01	delta_min as share of the interval of evaluation
	D_MAX	0.12	delta_max as share of the interval of evaluation
	INT_MIN	0.80	Minimum overlap of the interval
	K_V	10	Transition between ratings of 1 and 0 of the progression rating
	K_G	1	Transition between ratings of 1 and 0 of the size rating
	K_P	1	Transition between ratings of 1 and 0 of the phase shift rating
	G_V	0.50	Weighting factors of the progression rating
	G_G	0.25	Weighting factors of the size rating
	G_P	0.25	Weighting factors of the phase shift rating
	G_2	0.50	Weighting factors of the cross-correlation method

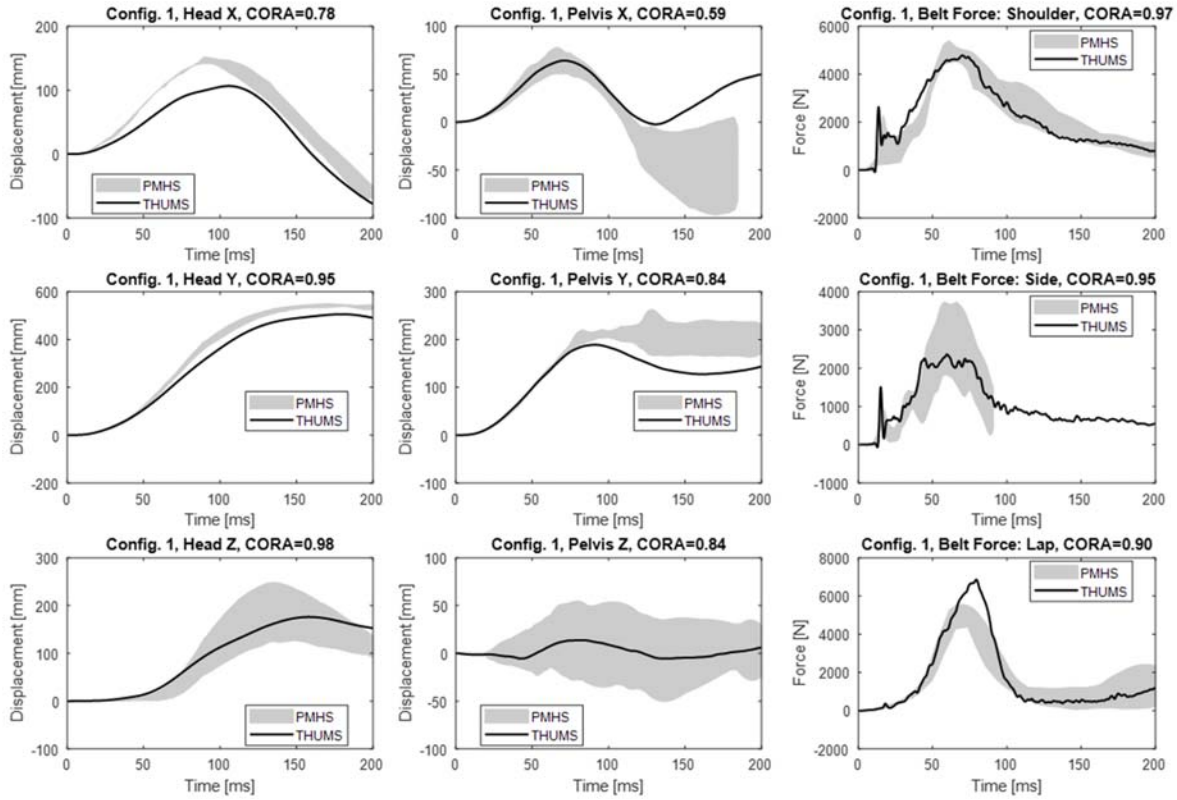

Fig. D.1. PMHS corridors, THUMS prediction and individual signal CORA rating. Head and Pelvis X-, Y-, Z-displacement and belt forces in configuration 1.

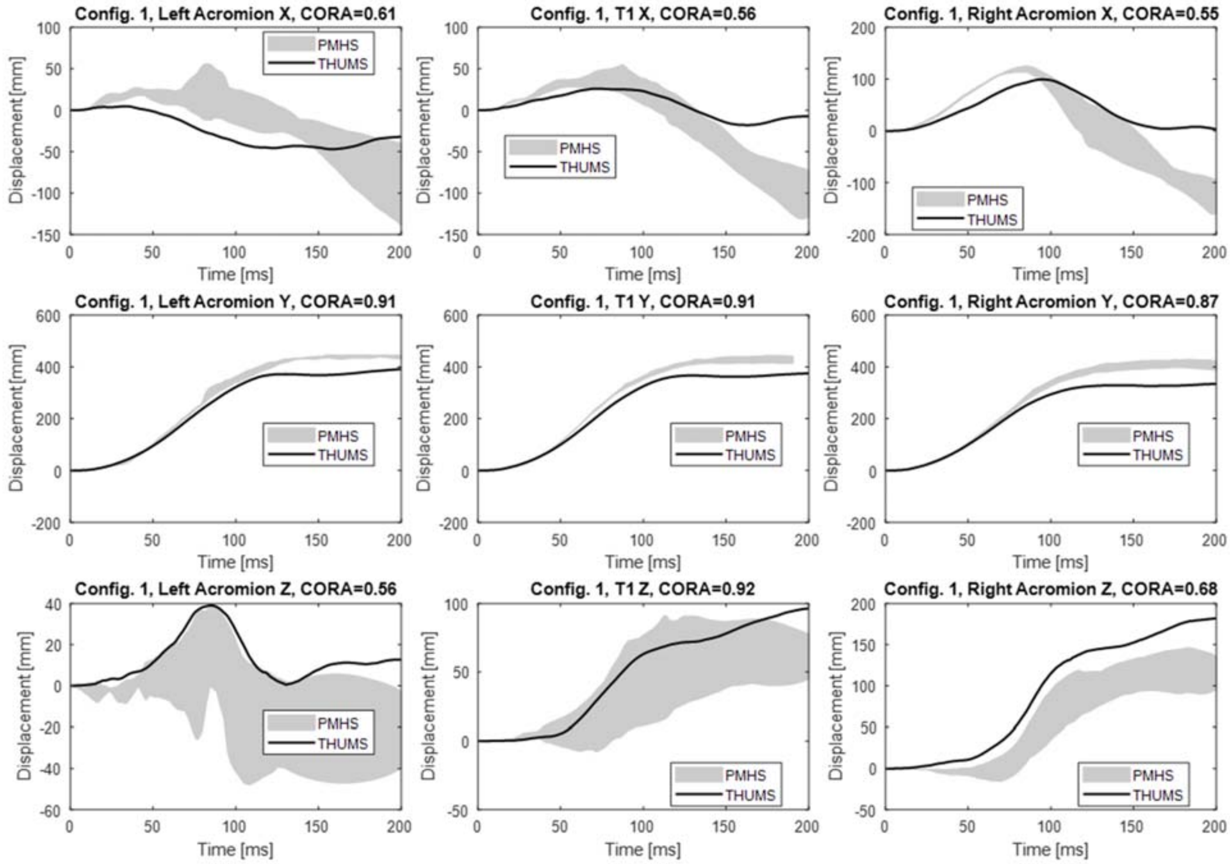

Fig. D.2. PMHS corridors, THUMS prediction and individual signal CORA rating. T1, Left and Right Acromion X-, Y-, Z-displacement in configuration 1.

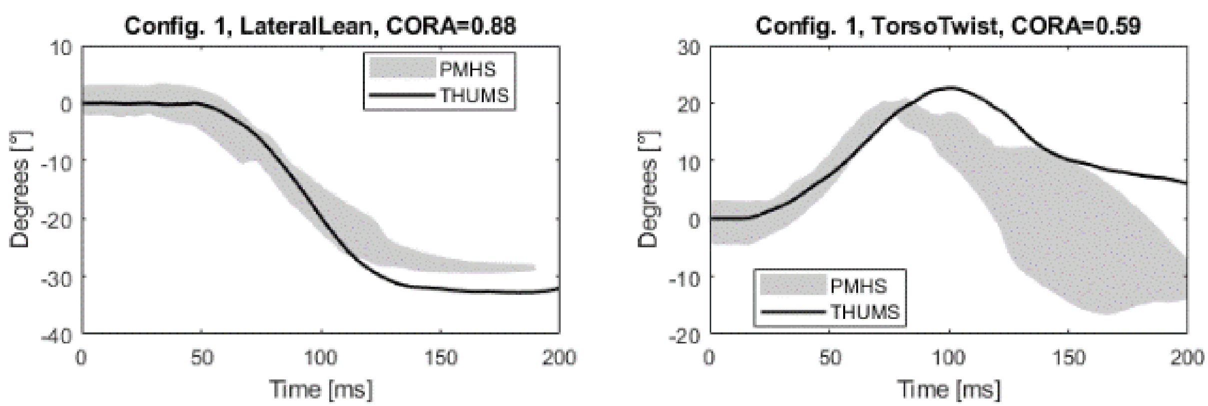

Fig. D.3. PMHS corridors, THUMS prediction and individual signal CORA rating. Lateral Lean and Torso Twist in configuration 1.

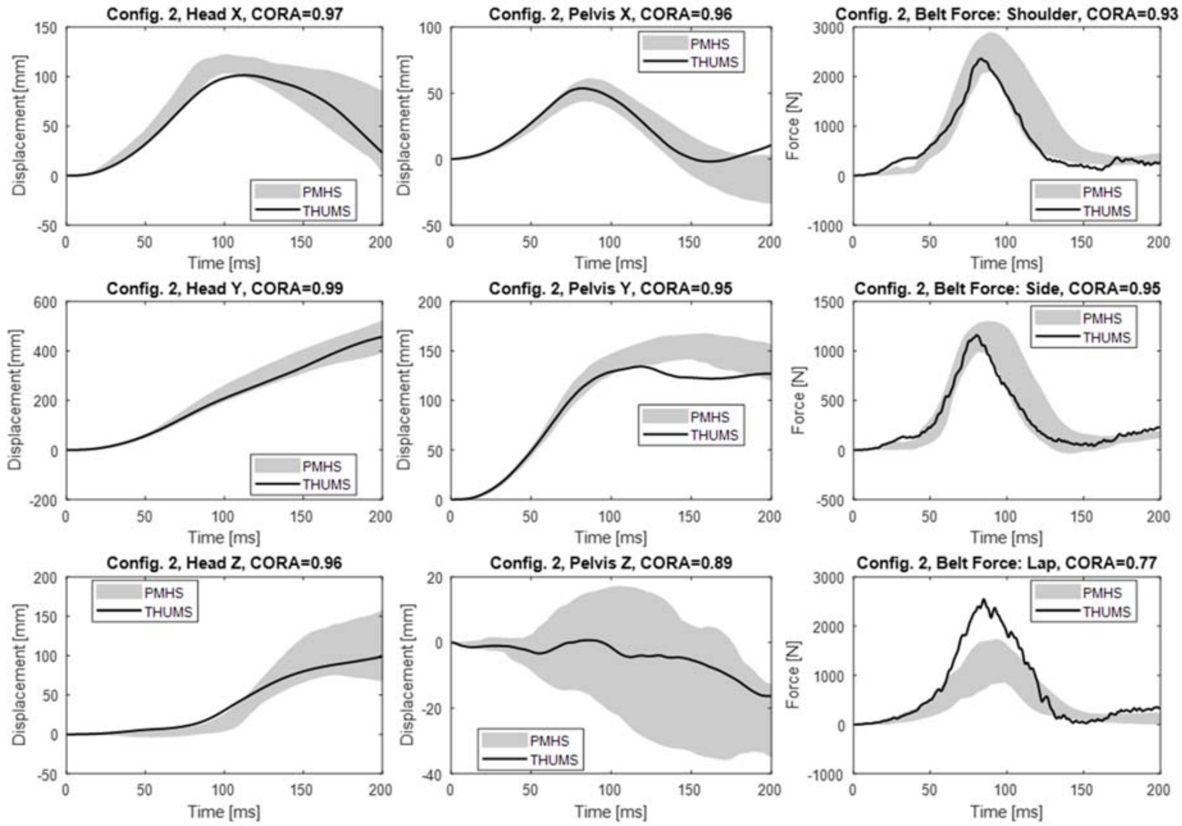

Fig. D.4. PMHS corridors, THUMS prediction and individual signal CORA rating. Head and Pelvis X-, Y-, Z-displacement and belt forces in configuration 2.

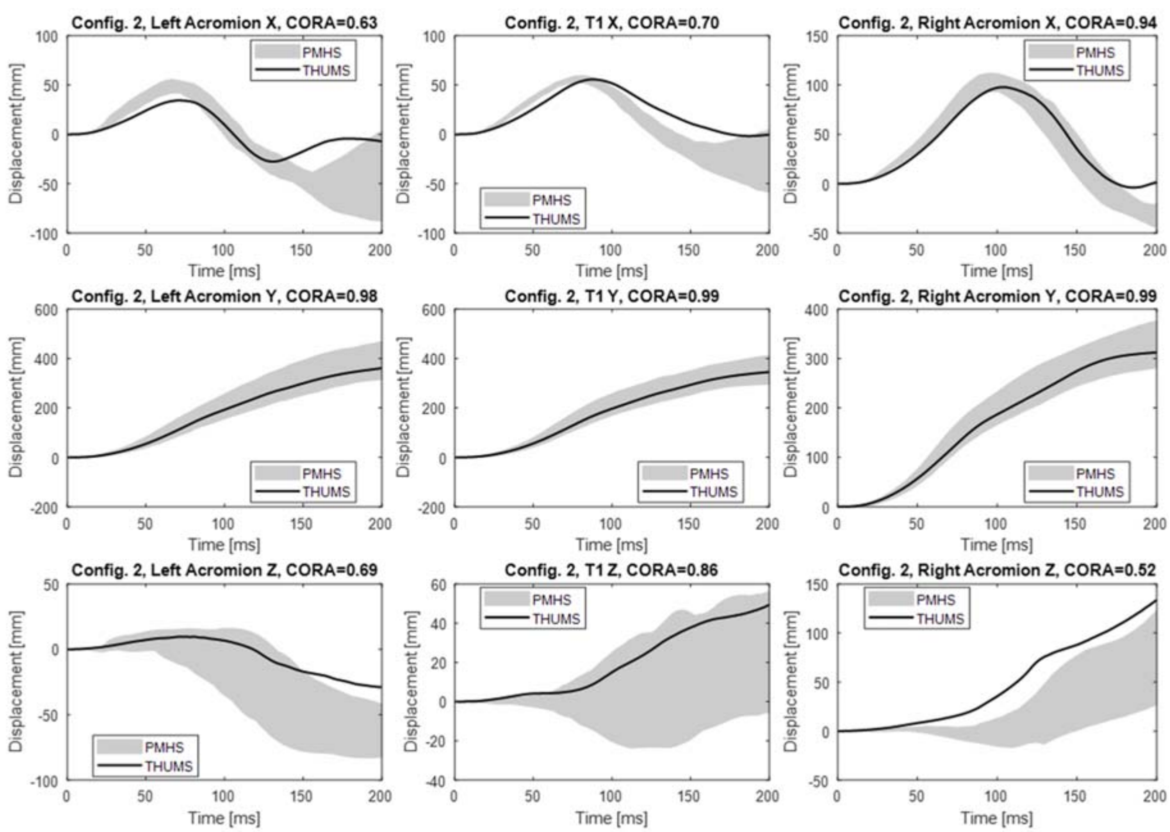

Fig. D.5. PMHS corridors, THUMS prediction and individual signal CORA rating. T1, Left and Right Acromion X-, Y-, Z- displacement in configuration 2.

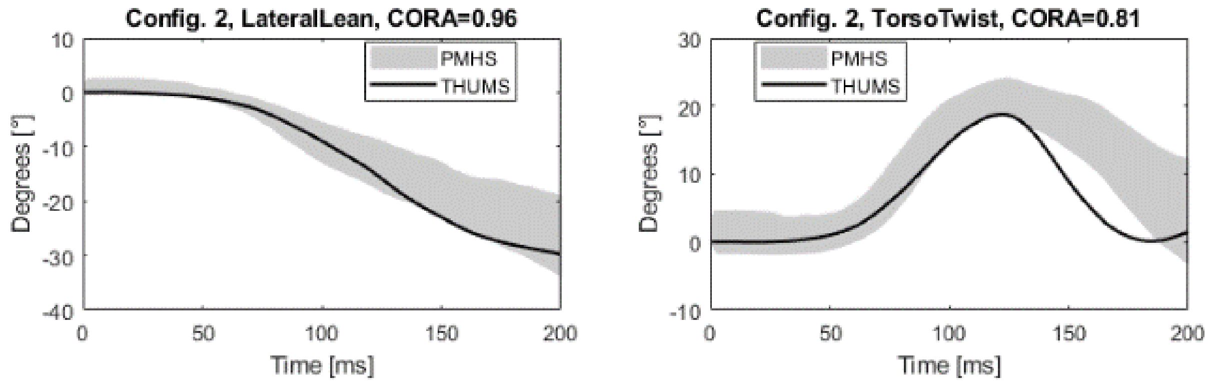

Fig. D.6. PMHS corridors, THUMS prediction and individual signal CORA rating. Lateral Lean and Torso Twist in configuration 2.

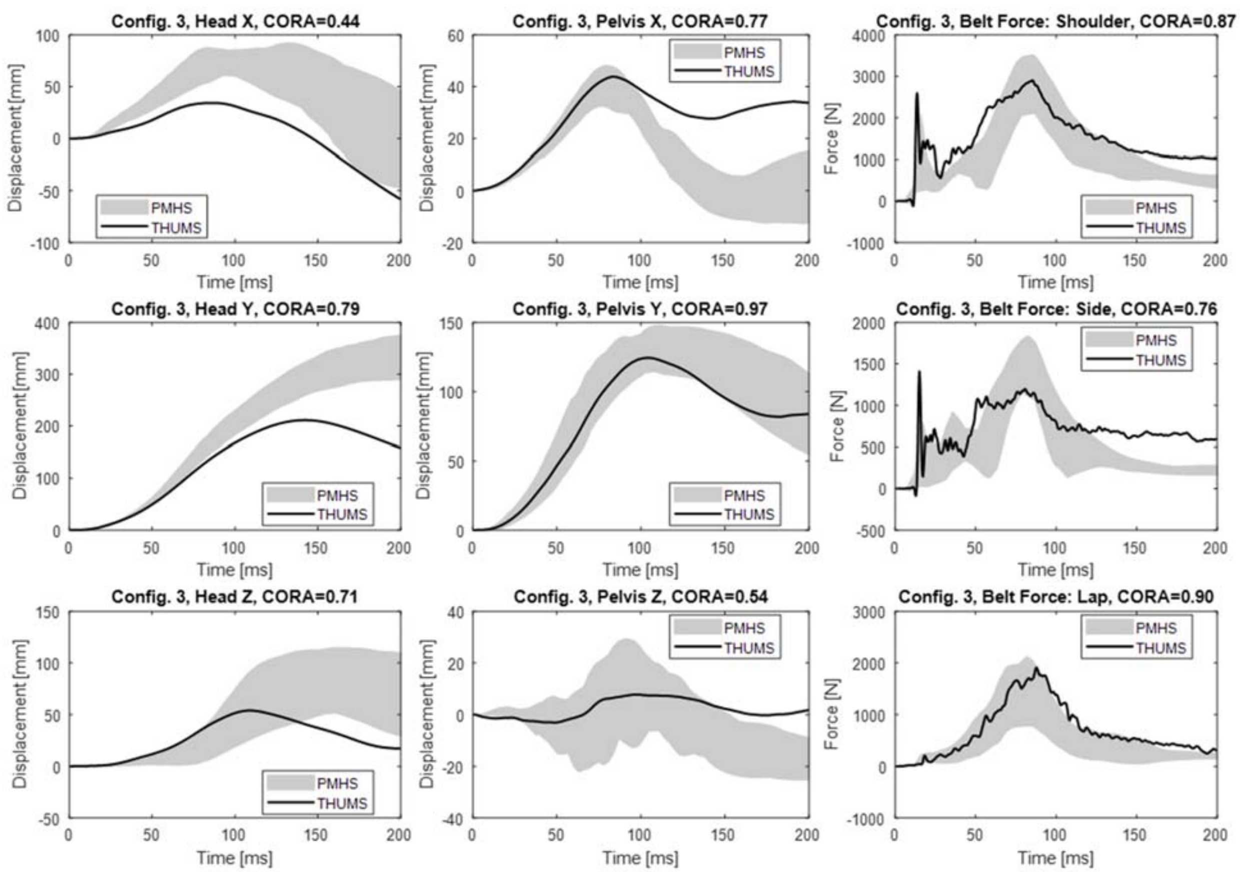

Fig. D.7. PMHS corridors, THUMS prediction and individual signal CORA rating. Head and Pelvis X-, Y-, Z-displacement and belt forces in configuration 3.

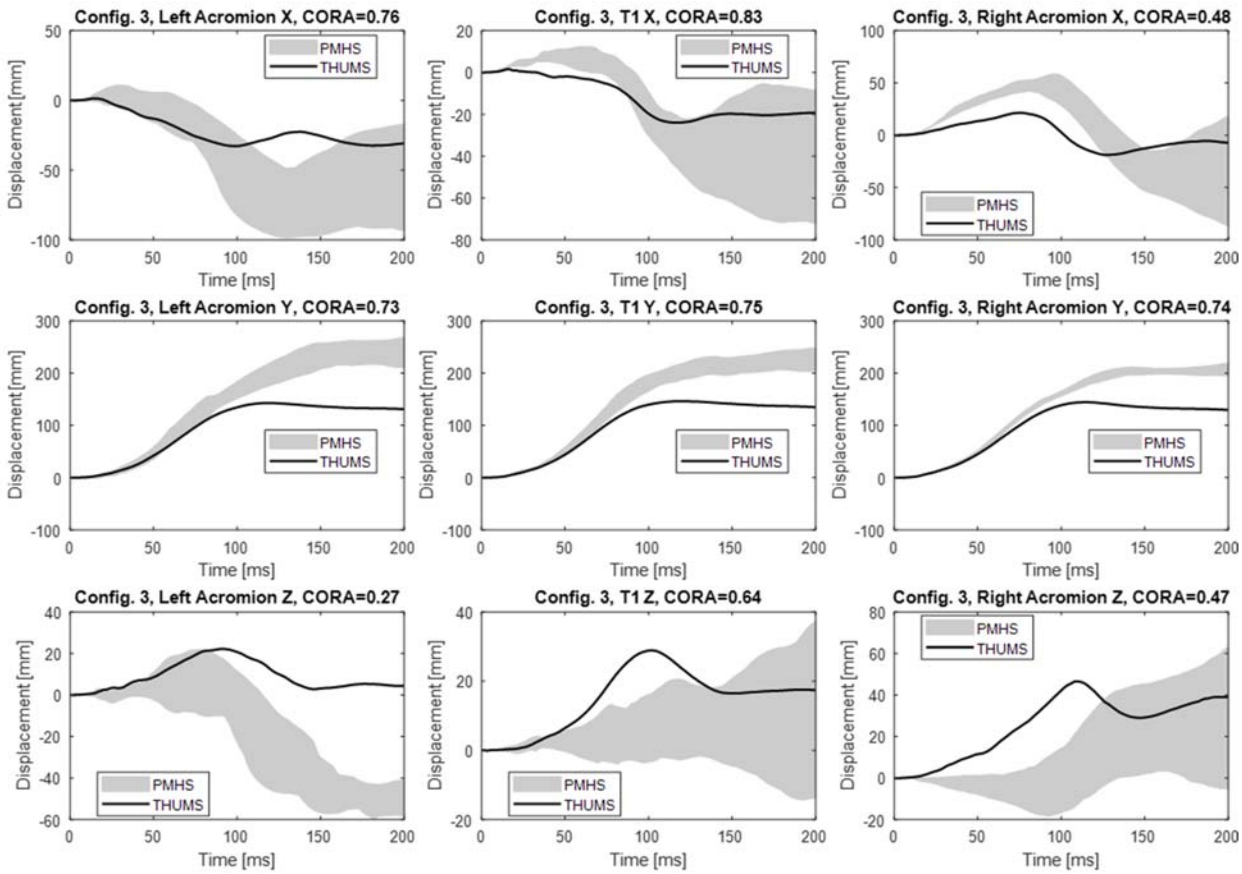

Fig. D.8. PMHS corridors, THUMS prediction and individual signal CORA rating. T1, Left and Right Acromion X-, Y-, Z- displacement in configuration 3.

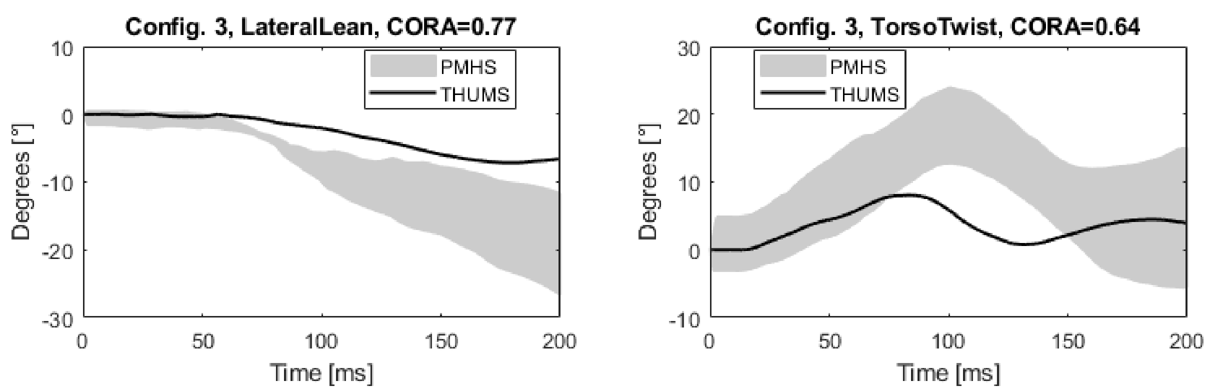

Fig. D.9. PMHS corridors, THUMS prediction and individual signal CORA rating. Lateral Lean and Torso Twist in configuration 3.

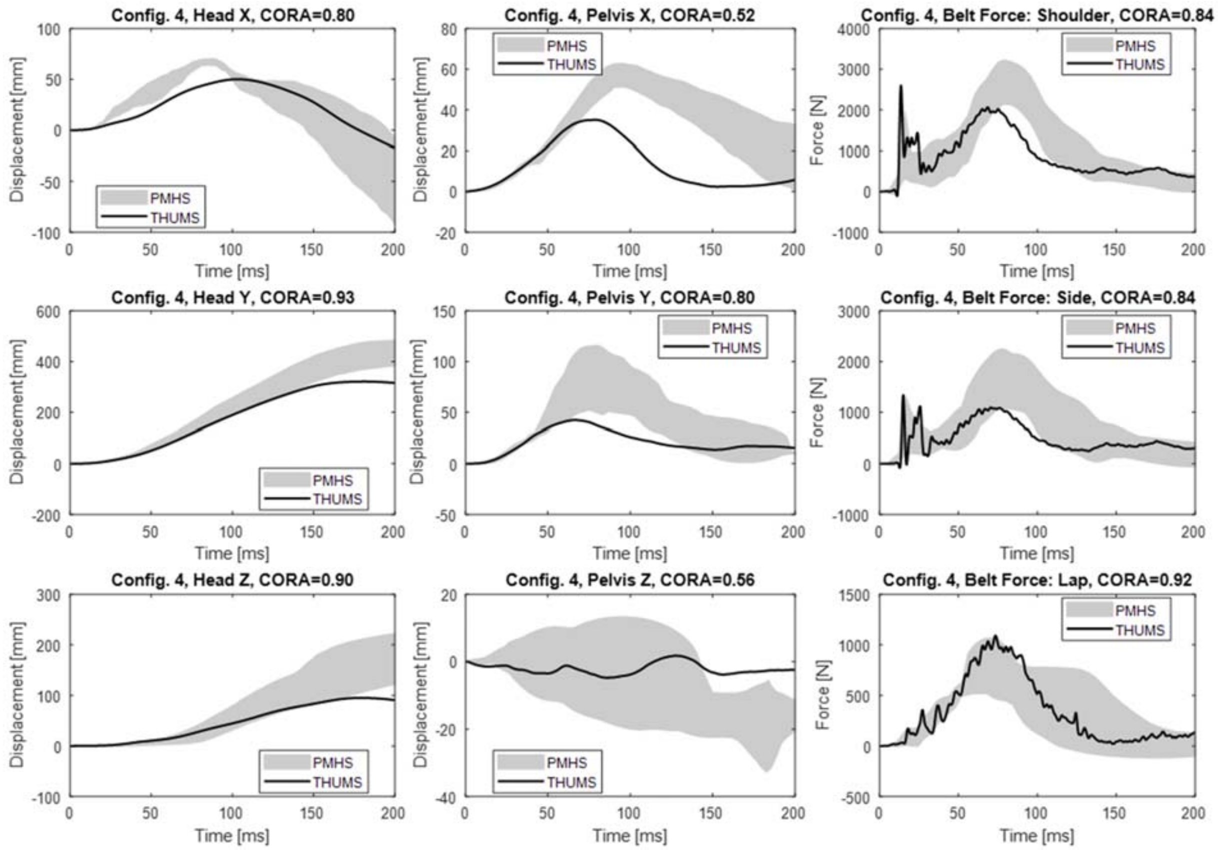

Fig. D.10. PMHS corridors, THUMS prediction and individual signal CORA rating. Head and Pelvis X-, Y-, Z-displacement and belt forces in configuration 4.

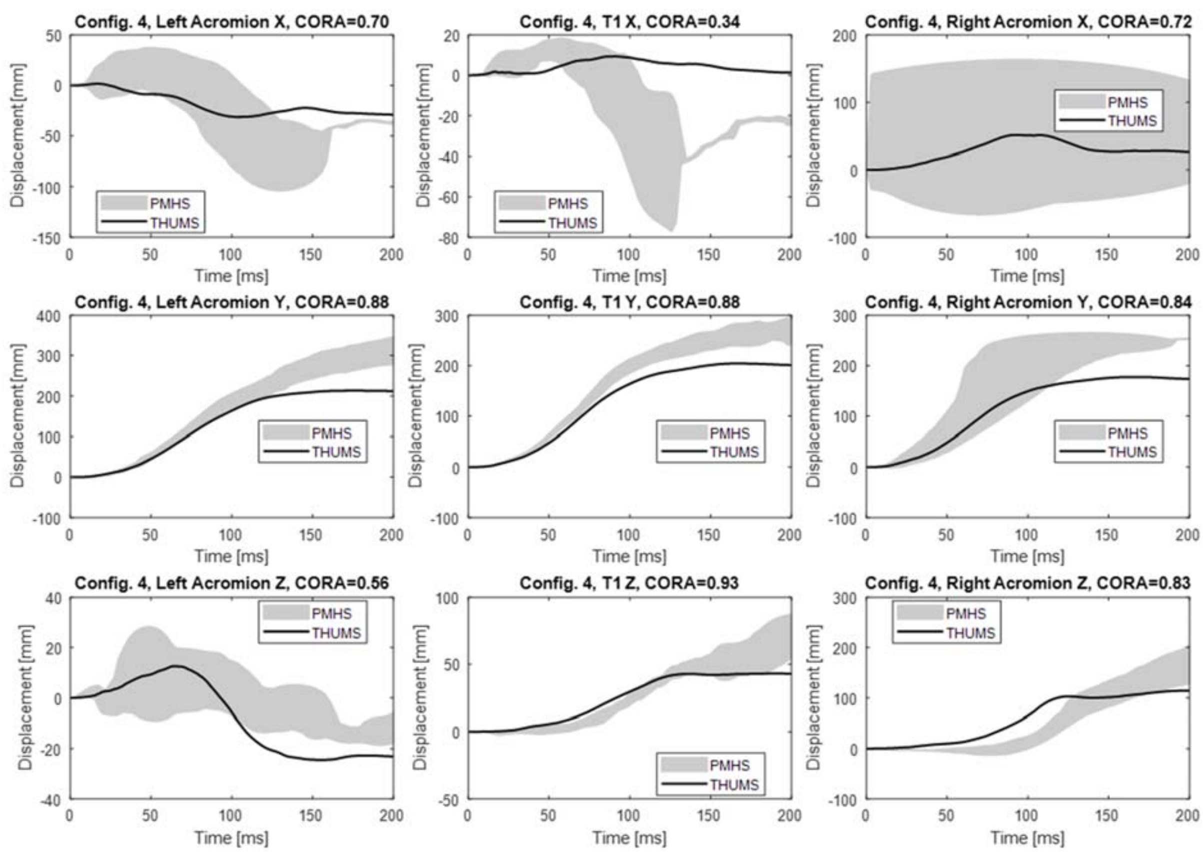

Fig. D.11. PMHS corridors, THUMS prediction and individual signal CORA rating. T1, Left and Right Acromion

X-, Y-, Z-displacement in configuration 4.

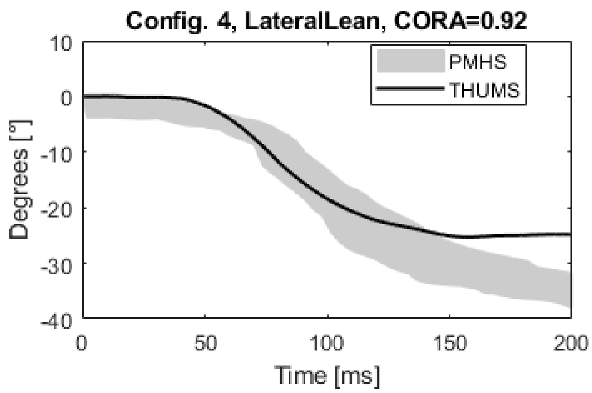

Fig. D.12. PMHS corridors, THUMS prediction and individual signal CORA rating. Lateral Lean and Torso Twist in configuration 4.

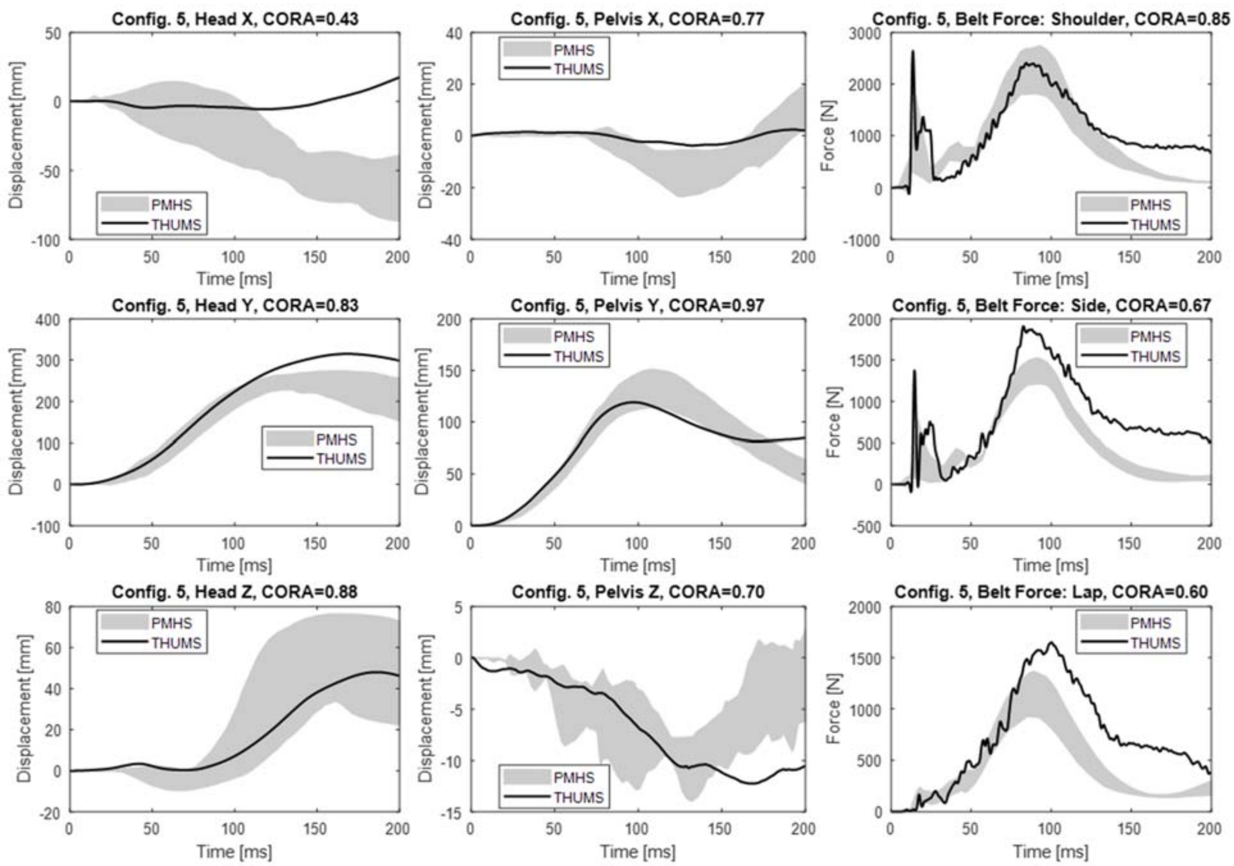

Fig. D.13. PMHS corridors, THUMS prediction and individual signal CORA rating. Head and Pelvis X-, Y-, Z-displacement and belt forces in configuration 5.

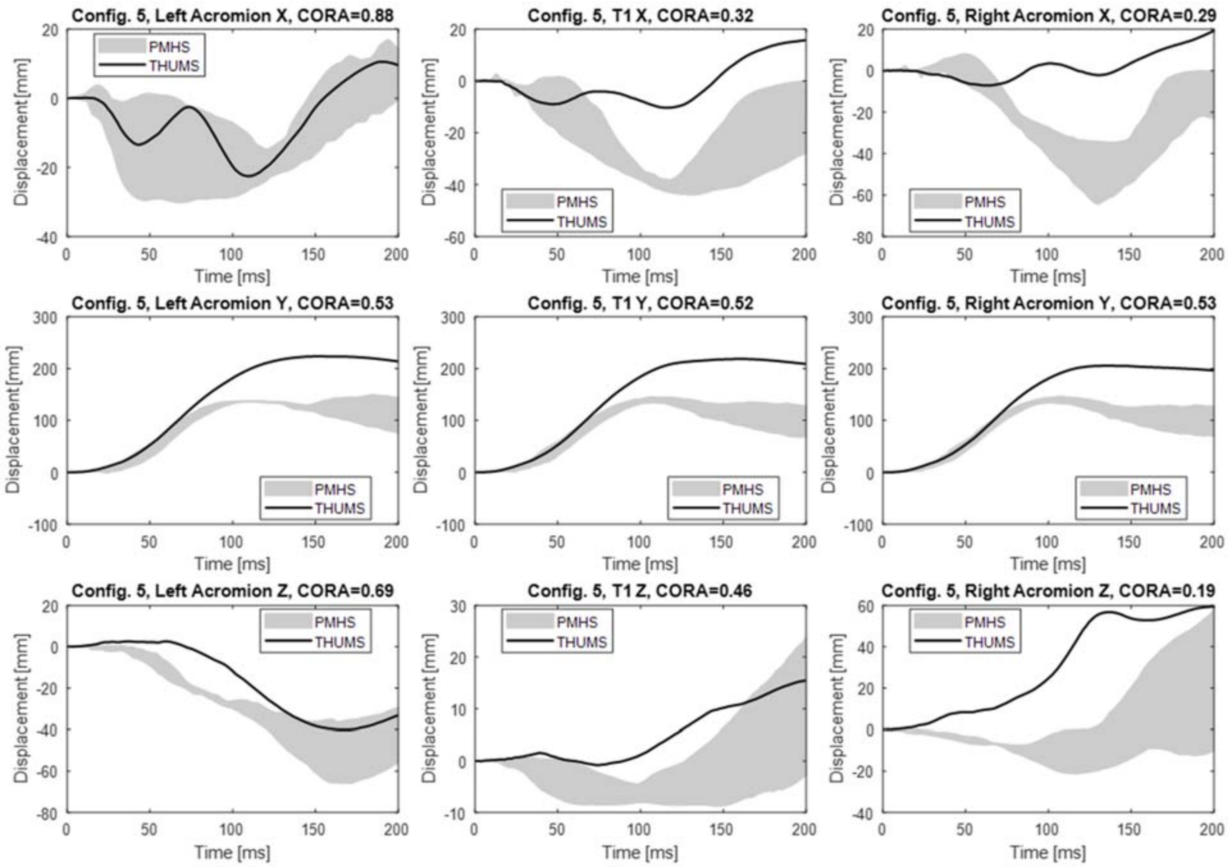

Fig. D.14. PMHS corridors, THUMS prediction and individual signal CORA rating. T1, Left and Right Acromion X-, Y-, Z- displacement in configuration 5.

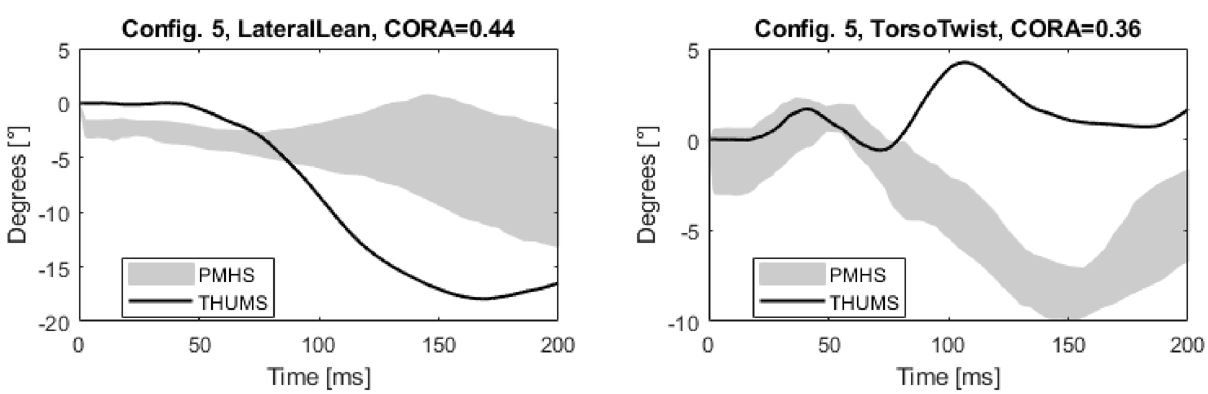

Fig. D.15. PMHS corridors, THUMS prediction and individual signal CORA rating. Lateral Lean and Torso Twist in configuration 5.

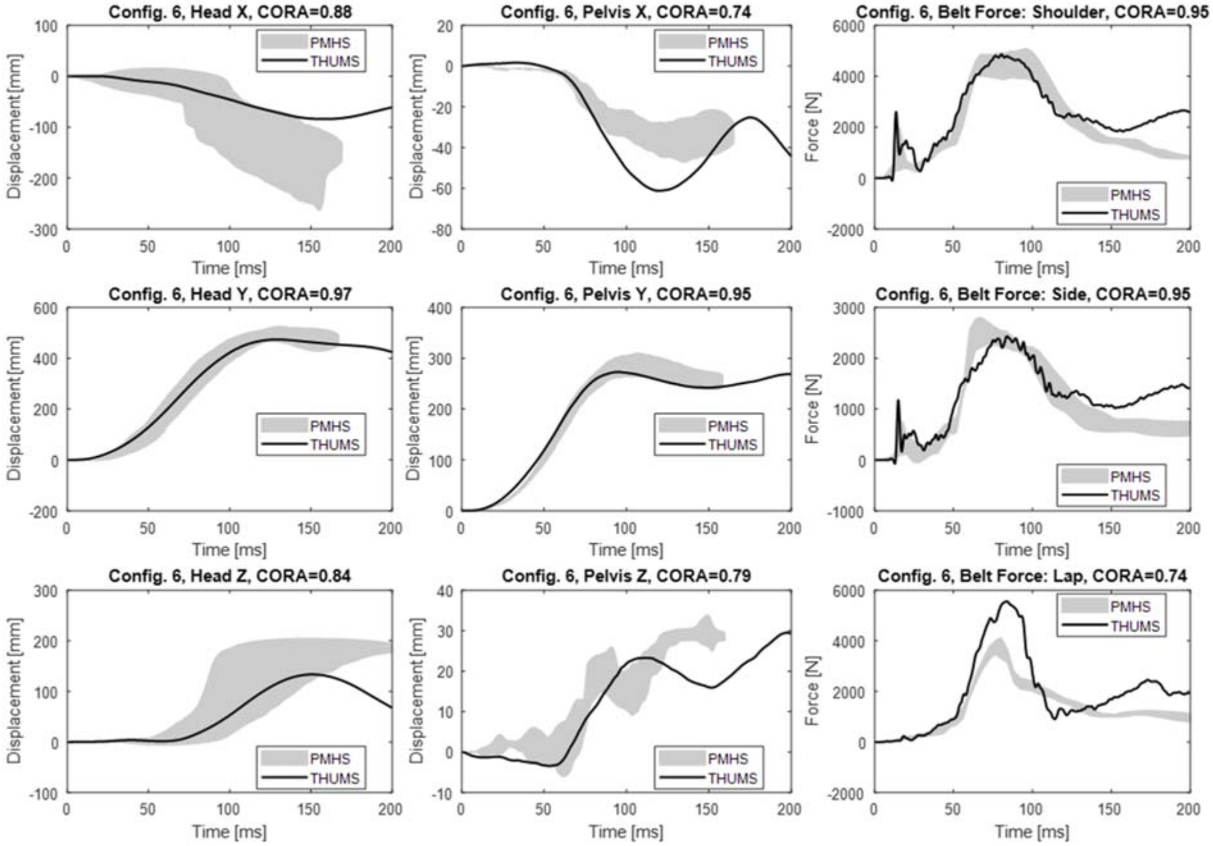

Fig. D.16. PMHS corridors, THUMS prediction and individual signal CORA rating. Head and Pelvis X-, Y-, Z-displacement and belt forces in configuration 6.

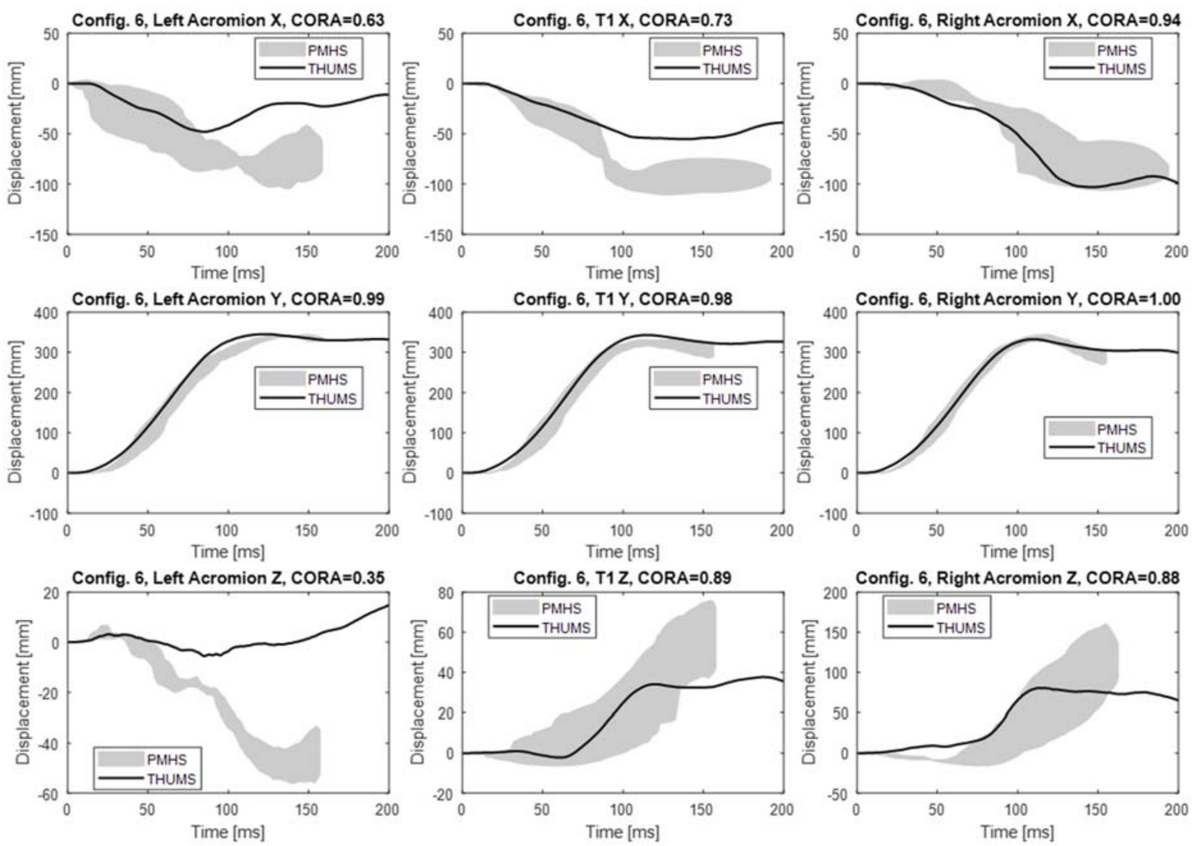

Fig. D.17. PMHS corridors, THUMS prediction and individual signal CORA rating. T1, Left and Right Acromion

X-, Y-, Z- displacement in configuration 6.

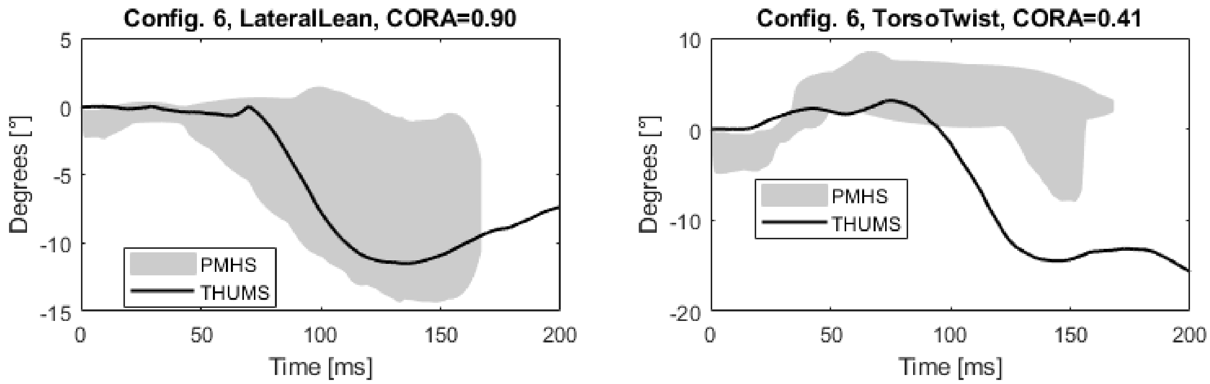

Fig. D.18. PMHS corridors, THUMS prediction and individual signal CORA rating. Lateral Lean and Torso Twist in configuration 6.

E. Peak Strain from Each Rib Cortical Bone in Far-Side Airbag Robustness Simulations

Maximum principal strain located in each rib cortical bone of the THUMS model during the robustness simulations is presented in Figures Fig. E.1-Fig. E.6 for AE-MDB impact in 90° to 15° with and without far-side airbag.

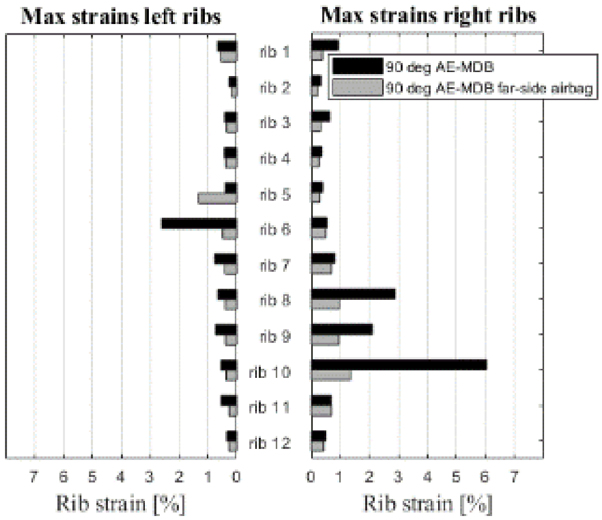

Fig. E.1. Peak rib cortical bone principal strain in 90° AE-MDB-to-vehicle simulation, with and without far-side airbag.

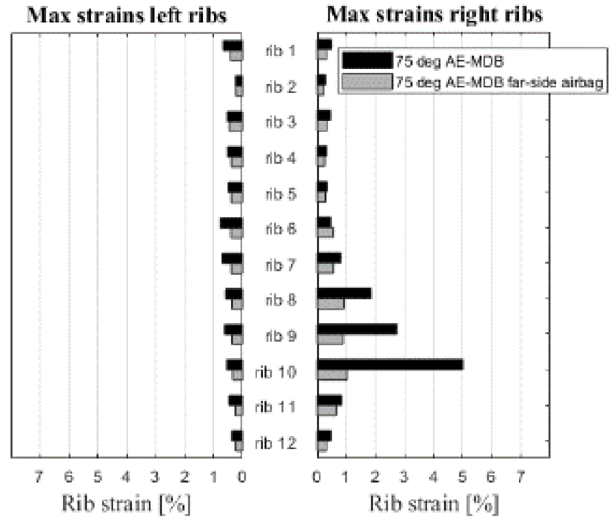

Fig. E.2. Peak rib cortical bone principal strain in 75° AE-MDB-to-vehicle simulation, with and without far-side airbag.

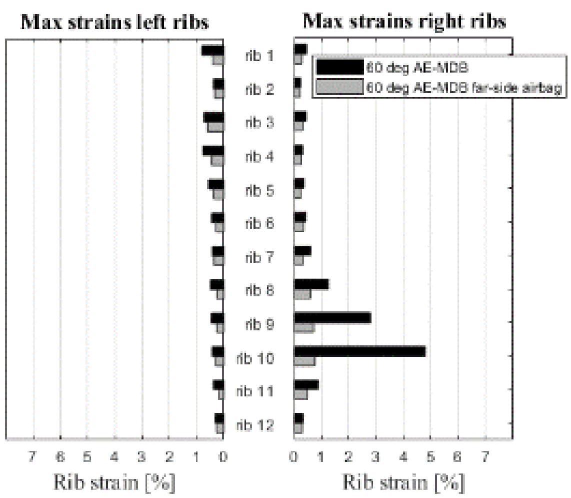

Fig. E.3. Peak rib cortical bone principal strain in 60° AE-MDB-to-vehicle simulation, with and without far-side airbag.

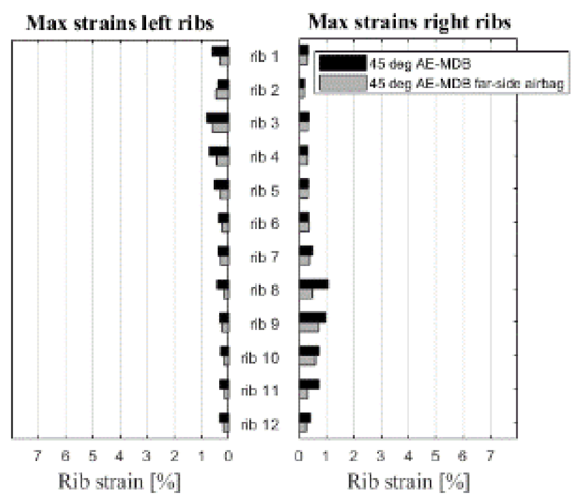

Fig. E.4. Peak rib cortical bone principal strain in 45° AE-MDB-to-vehicle simulation, with and without far-side airbag.

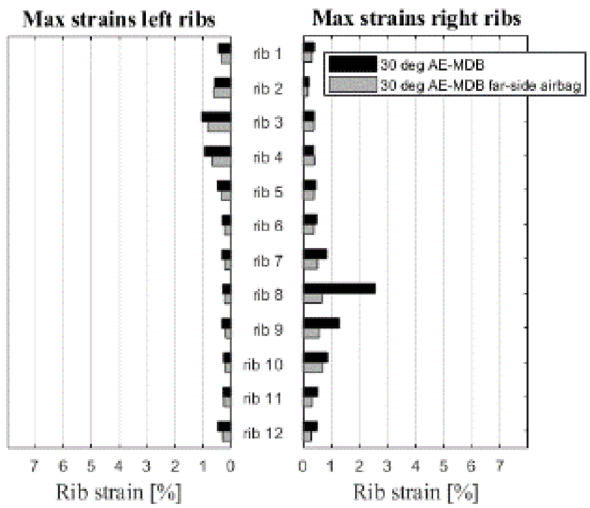

Fig. E.5. Peak rib cortical bone principal strain in 30° AE-MDB-to-vehicle simulation, with and without far-side airbag.

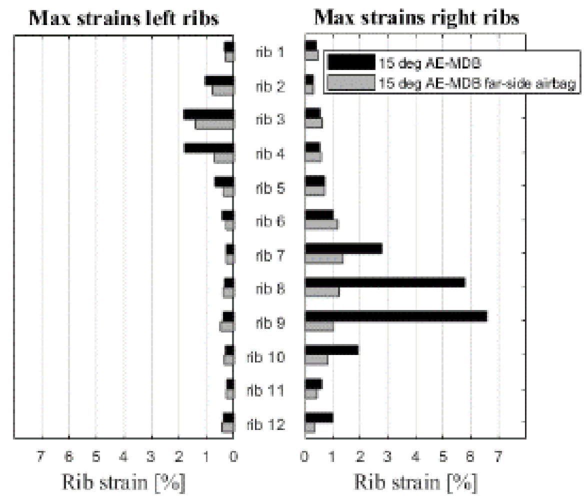

Fig. E.6. Peak rib cortical bone principal strain in 15° AE-MDB-to-vehicle simulation, with and without far-side airbag.

F. Modifications to the THUMS model

Body Part		**Modification**
Chest	**Ribs**	**Geometry and mesh modified** "Shi X, Cao L, Reed MP, Rupp JD, Hoff CN, Hu J. (2014) A statistical human rib cage geometry model accounting for variations by age, sex, stature and body mass index. *Journal of biomechanics. 2014;47(10): pp. 2277-2285.*" **Cortical bone thickness modified** "Choi H-Y, Kwak D-S. (2011) Morphologic Characteristics of Korean Elderly Rib. J. Automot. Saf. Energy. 2011;2" **Cortical bone properties modified** "Kemper AR, McNally C, Kennedy EA, *et. al*. (2005) Material properties of human rib cortical bone from dynamic tension coupon testing. *Stapp car crash journal. 2005;49: pp. 199-230.* "Kemper AR, McNally C, Pullins CA, Freeman LJ, Duma SM, Rouhana SM. The biomechanics of human ribs: material and structural properties from dynamic tension and bending tests. *Stapp car crash journal. 2007;51: pp. 235-273*."
Lumbar Spine	**Vertebra**	**Remeshed** Contact between vertebra and intervertebral disk added Intervertebral ligaments modified – both geometry and properties "Afwerki, H. (2016) Biofidelity Evaluation of Thoracolumbar Spine Model in THUMS. Master's Thesis in Biomedical Engineering, *Chalmers University of Technology, 2016*"
Head		**New Head Model** "Kleiven, S. (2007). Predictors for Traumatic Brain Injuries Evaluated through Accident Reconstructions. *51st Stapp Car Crash Journal,2007: pp. 81-114.*"